Origin of volcanic-hosted Mn-oxide mineralization from San Pietro Island (SW Sardinia, Italy): An integrated geochemical, mineralogical

Contents lists available at ScienceDirect

Journal of Geochemical Exploration

journal homepage: www.elsevier.com

Origin of volcanic-hosted Mn-oxide mineralization from San Pietro Island (SW Sardinia, Italy): An integrated geochemical, mineralogical and isotopic study

E. Pitzalis [a], P. Fulignati [a, *], M. Lezzerini [a], R. Cioni [b], L. Pinarelli [c], M. Tamponi [a], A. Gioncada [a]

[a] Department of Earth Sciences, University of Pisa, via S. Maria 53, 56126 Pisa, Italy
[b] Department of Earth Sciences, University of Florence, via La Pira 4, 50121 Firenze, Italy
[c] Institute of Geosciences and Earth Resources, Section of Florence, National Research Council (CNR), via La Pira 4, 50121 Florence, Italy

ARTICLE INFO

Keywords:
Mn-ore
Volcanic-hosted
Mineralizing fluids
REE
Pb isotopes
Sardinia

ABSTRACT

The Mn-oxide mineralizations from Sardinia (Italy) represent examples of Mn deposits in a continental environment and, as such, their investigation can shed light on the genesis and characteristics of this deposit type, less studied than their more common oceanic counterpart. In this paper, the genetic mechanisms, the physical-chemical conditions and the origin of the mineralizing fluids are discussed for the volcanic-hosted Mn ores of the San Pietro Island (SW Sardinia), through an integrated geochemical, mineralogical and radiogenic isotope approach. New and published data are here examined on the basis of recent trace element discrimination schemes for Mn ores and a model for the genesis is proposed.

The mineralogy of the alteration paragenesis (argillic facies) and the type of observed fluid inclusions (very small monophase liquid inclusions) suggest a circulation of mineralizing fluids characterized by weak acidic conditions (pH indicatively around 5) and relatively low temperature (< 100–120 °C). Geochemical features such as the contents of transition metals (Mn, Fe, Cu, Co, Ni, Zn), and contents and ratios of rare-earth elements and yttrium (REY), suggest that the San Pietro Island Mn metallogenesis is the result of combined hydrothermal and hydrogenetic mechanisms of formation. The Pb isotope compositions of different Mn veins exhibit a significant spread that suggests the contribution of distinct mineralizing fluids, deriving their isotopic signature from both seawater and water-rock interaction processes.

The possible model of formation of the San Pietro Mn mineralization can be viewed as a complex process, in which Mn-bearing fluids originated from remobilization of Mn oxides sequestered in shelf and slope sediments and/or by leaching of the older Cenozoic volcanic rocks that form the basement of the island. Fluid rise was due to hydrothermal convection, possibly related to the general thermal anomaly active in the area from 15 to 12 My, during the final stage of the intense Cenozoic volcanic activity of the Sulcis area (San Pietro, Sant'Antioco, Isola del Toro volcanic activity). The fluids were probably dominated by seawater, characterized by relatively low temperatures and acidic conditions, due to the input of H_2S of hydrothermal origin. The Mn ore deposition occurred in relatively shallow water and oxidizing environment, following the pH neutralization induced by water-rock interaction processes.

1. Introduction

Since prehistoric times, Sardinia Island (Italy) has been the locus of an intense mining activity. The large variety of its deposits spans from the relevant polymetallic Pb-Zn hydrothermal (SEDEX, Mississippi-Valley-type) to epithermal (low and high sulfidation) mineralization to polymetallic skarns, and include raw materials for ceramic and glass industries, ornamental stones, coal and bauxite mines (e.g., Boni et al., 1996; Ruggieri et al., 1997; Palomba et al., 2006). Important Mn oxide mineralization, also, occur in the northwestern and southwestern portions of the island (Guerin, 1983; Sinisi et al., 2012). These Mn deposits include both sediment-hosted (Mt. Jorzi, Ittiri-Uri, Padria areas - NW Sardinia) and volcanic-hosted (Anglona area - NW Sardinia and San Pietro Island - SW Sardinia) types, interpreted by previous studies

* Corresponding author.
Email address: paolo.fulignati@unipi.it (P. Fulignati)

https://doi.org/10.1016/j.gexplo.2019.05.010
Received 22 January 2019; Received in revised form 30 April 2019; Accepted 28 May 2019
Available online xxx
0375-6742/

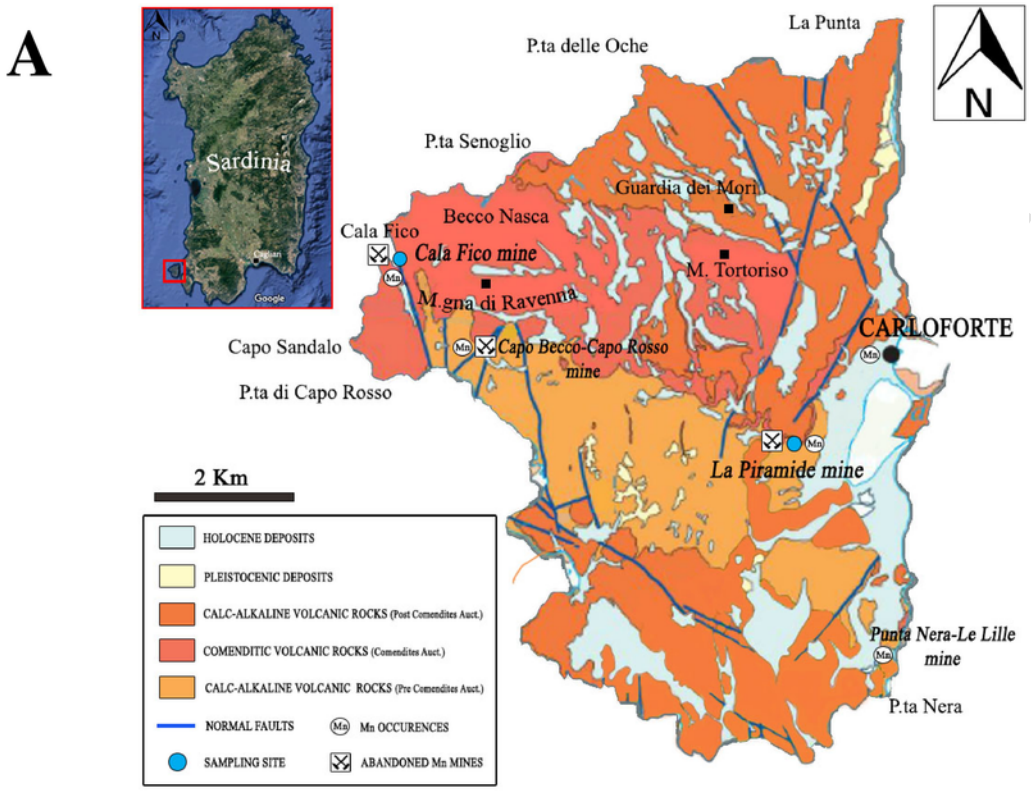

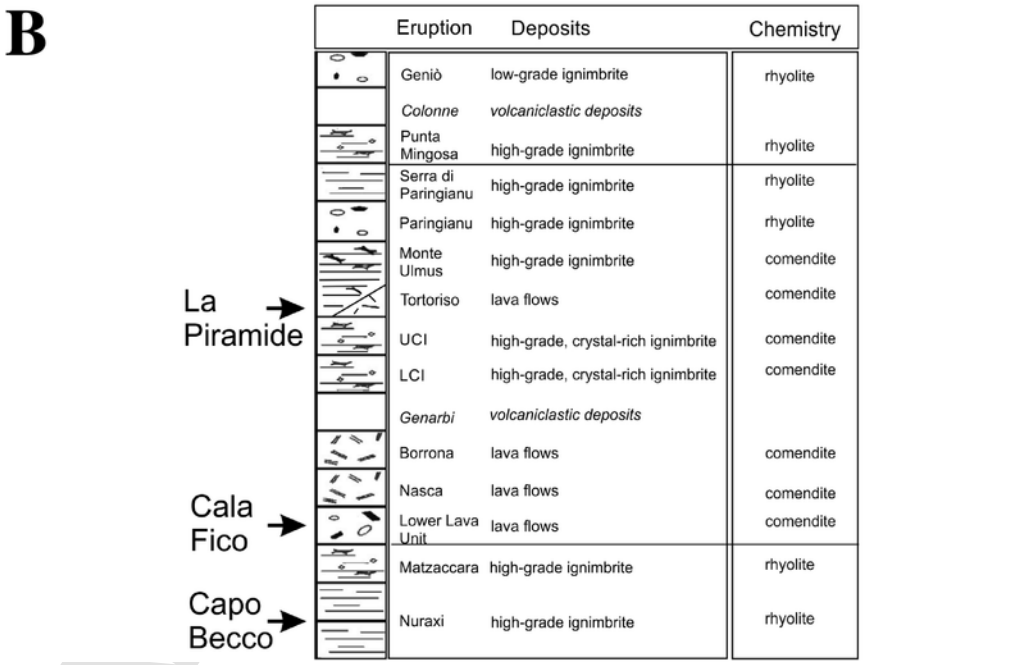

Fig. 1. A. Simplified geological map of San Pietro Island (modified after Botta et al., 2015). The sampling sites (mines of *La Piramide* and *Cala Fico*) are indicated. B. Stratigraphic scheme correlating the volcanic successions of the SPI and the Sulcis mainland with highlight of the sampling sites (modified from Cioni et al., 2001).

as diagenetic and hydrothermal (mixing of magmatic and meteoric waters) respectively (Sinisi et al., 2012; Mongelli et al., 2013). The Sardinian deposits are associated to a continental arc environment (Sinisi et al., 2012). While genetic mechanisms of Mn-ore in the oceanic environment are relatively well constrained (e.g. Nicholson, 1992; Xiao et al., 2017), few studies exist regarding the genesis of Mn mineralizations in the shallow marine/continental environment. In order to shed some light on the possible processes related to these deposits, this paper deals with the volcanic-hosted Mn-ores of the San Pietro Island, located in the southwestern part of Sardinia.

Here we applied an integrated geochemical, mineralogical and radiogenic isotope approach and used both new and available data from literature (Sinisi et al., 2012) to propose a constrained ore-forming model for Mn-oxide ores at San Pietro Island. In particular, geochem-

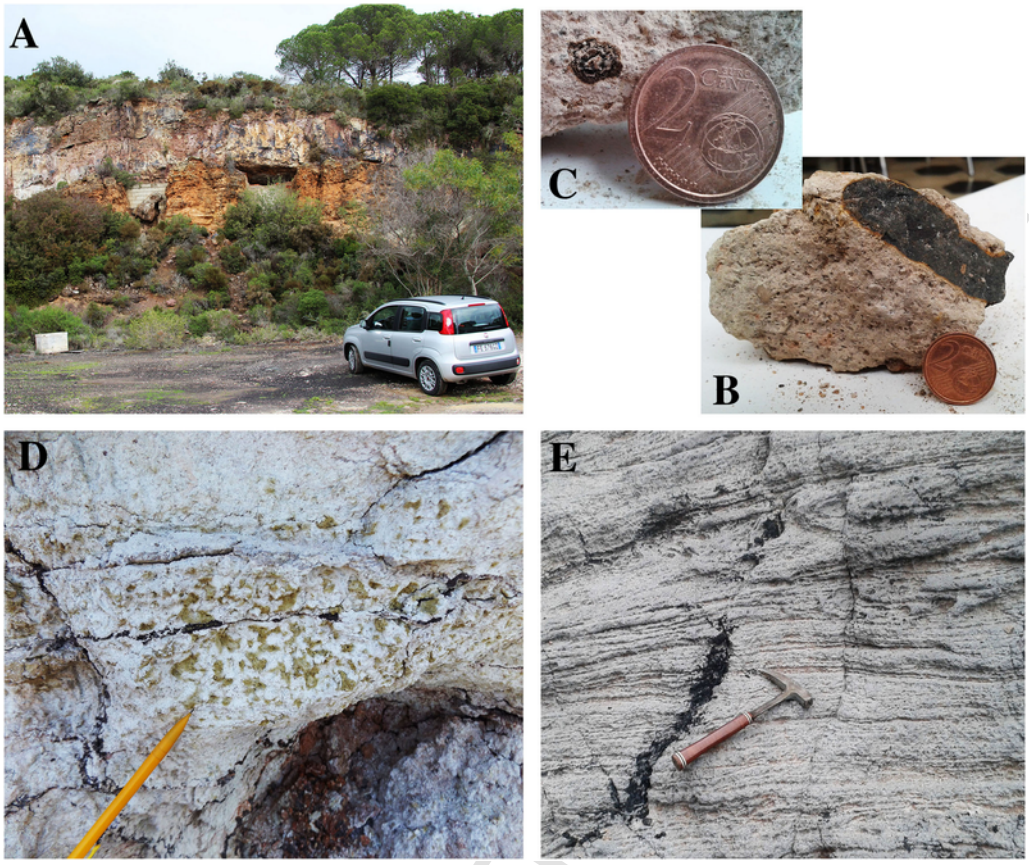

Fig. 2. A. Contact between the Upper Comenditic Ignimbrite (below) and the Monte Ulmus ignimbrite (above) at *La Piramide*. B. Mn ore vein within comenditic ignimbrite. C. Disseminated Mn spots ("ocelli") in the Upper Comenditic Ignimbrite. D. Argillified volcanics at *La Piramide*. E. Mn veins in the *Cala Fico* comenditic lava flow.

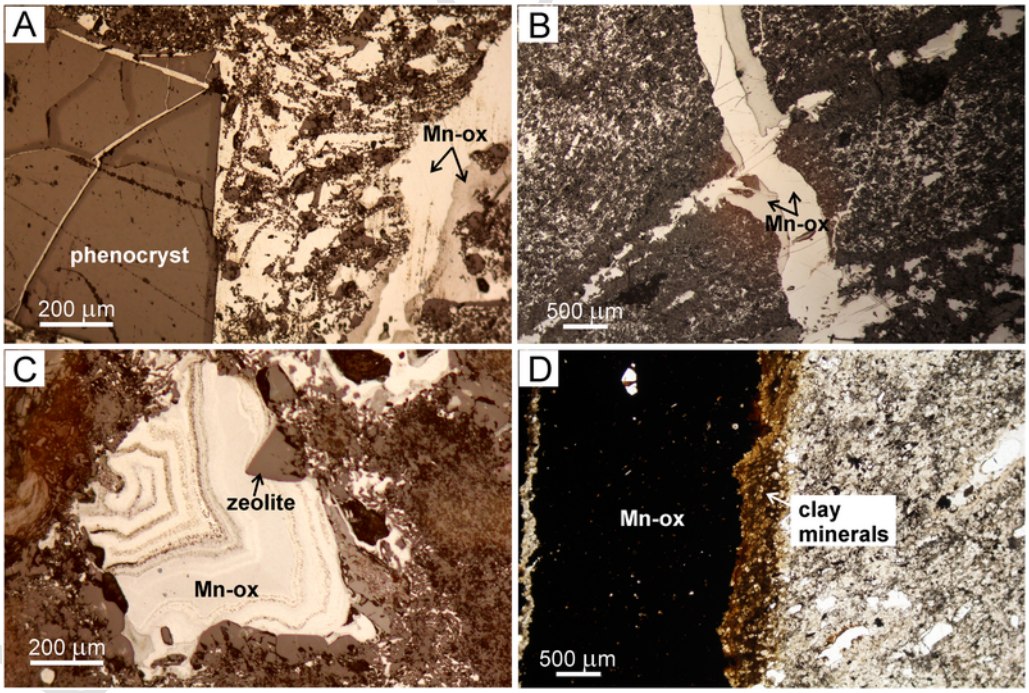

Fig. 3. A. Mn-oxide minerals filling cracks and rock porosity in the *La Piramide* ignimbrite host (reflected light, parallel nicols microphoto). B. Fracture-filling texture; note that two Mn minerals can be distinguished by the different reflectivity (reflected light, parallel nicols microphoto). C. Mn-oxide filling void in the ignimbrite, postdating zeolite minerals (reflected light, parallel nicols microphoto). D. Orange clay–rich boundary between the Mn ore vein and the host rock (transmitted light, parallel nicols microphoto).

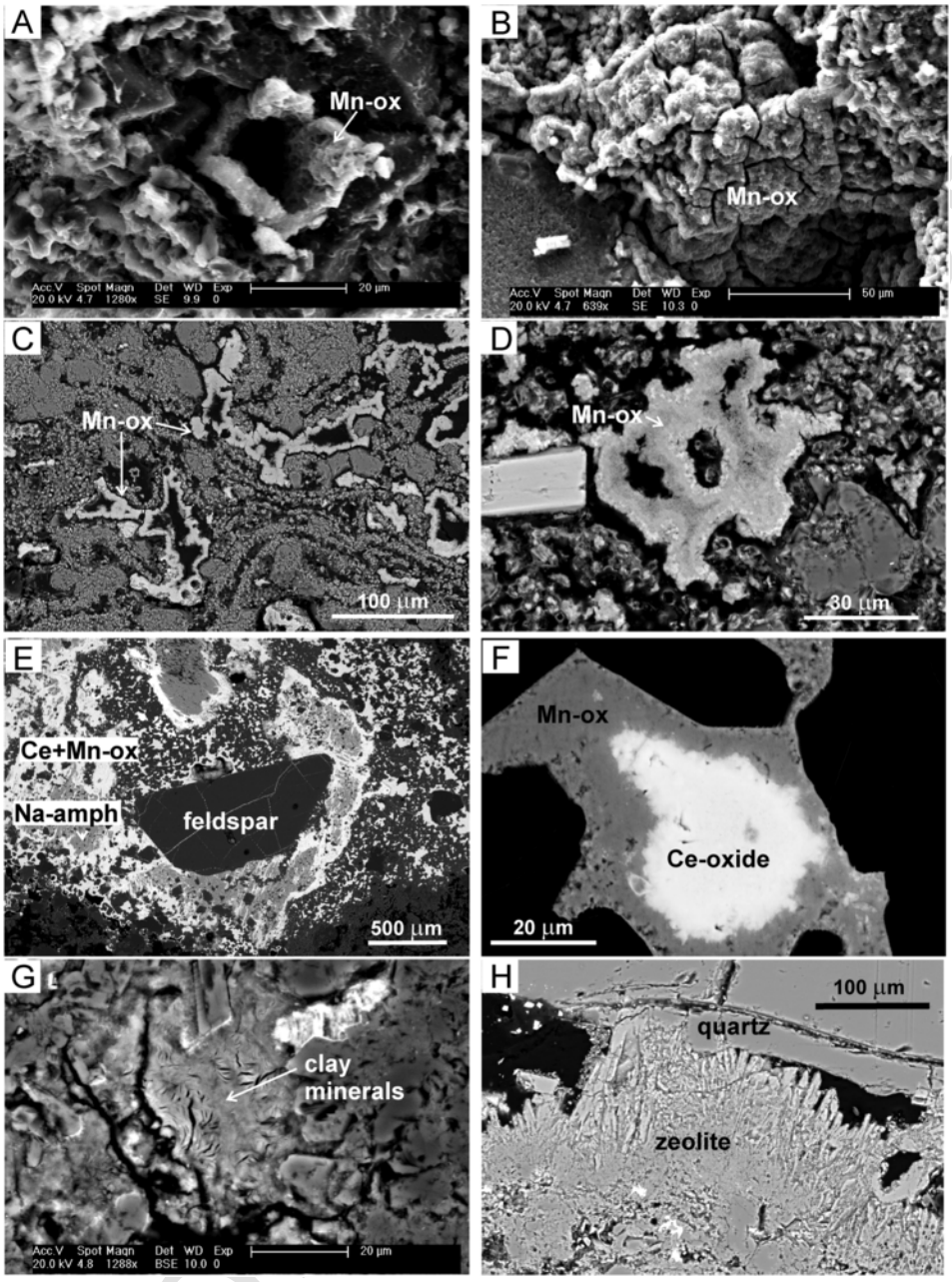

Fig. 4. A. Mn-oxide lining porosity between quartz and feldspar crystals in the ignimbrite (SE image). B. Mn-oxide concretions on quartz crystals (SE image). C, D. Mn-oxide mineralization filling open spaces in the host-rock matrix. Dark areas are formed by K-rich Mn oxide; light areas are formed by Ba-rich Mn oxide (BSE images). E. K-feldspar phenocryst surrounded by Mn mineralization. Brightest areas are due to the occurrence of micron-sized Ce oxides closely associated to Mn oxides (BSE image). F. Particular of Mn oxide mineralization with associated Ce-oxide enrichment (BSE image). G. Clay minerals (smectites) on the hydrothermally altered comenditic host rock (BSE image). H. Zeolites as alteration of the ignimbrite unit at La Piramide (BSE image).

istry of rare-earth elements (REE), recent trace element discrimination schemes for Mn ores (Bau et al., 2014; Josso et al., 2017), Pb isotope systematics, and mineralogy are employed to characterize the origin of the mineralizing fluids responsible of Mn-ore formation, and to trace the ore forming processes.

2. Geological setting

During the last 30 Ma, the Alpine orogenesis deeply controlled the geological evolution of the entire circum-Mediterranean area, including the Sardinia-Corsica block. During upper Oligocene-lower Miocene, the NNW-trending subduction of African oceanic lithosphere below the margin of the European continental plate triggered the opening of the Ligurian-Provençal back-arc basin (Beccaluva et al., 1994; Catalano et al., 2001; Speranza et al., 2002), thus starting the counter-clockwise rotation of the Sardinia-Corsica block, which definitively stopped in Langhian times (around 15 Ma) (Speranza et al., 2002).

Regional geodynamics culminated in two distinct igneous episodes (Oligo-Miocene and Plio-Quaternary), with a varied magmatic activity ranging in composition from subalkaline to strongly alkaline (Lustrino et al., 2004, 2013). The Oligo-Miocene volcanic activity (32–15 Ma) was linked to the development of a magmatic arc along the western margin of the Sardinia-Corsica microplate. The volcanic products (dacitic to rhyolitic ignimbrites with a subalkaline affinity) are mainly distributed over the central-western sector of the island along the "Fossa Sarda", a N-S to NW-SE graben-like structure that crosses Sar-

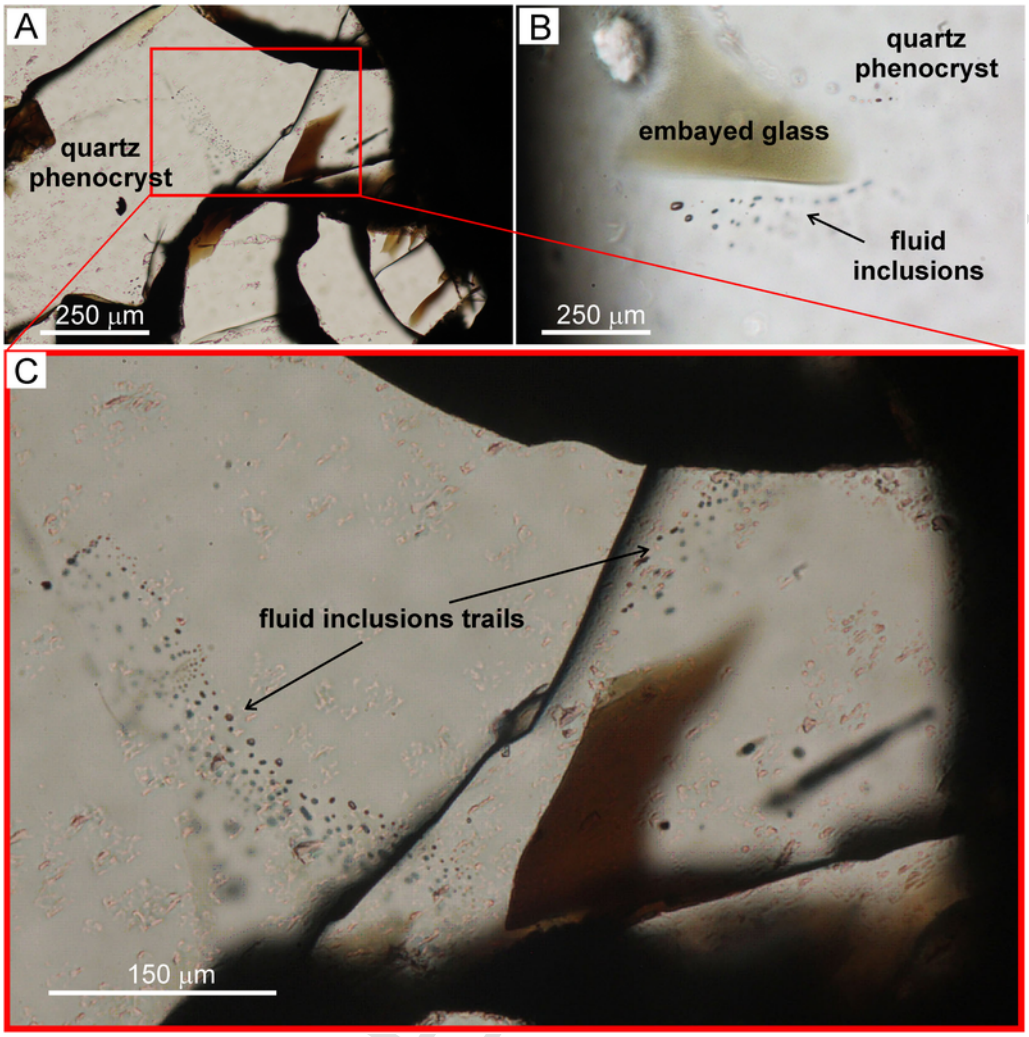

Fig. 5. A, B. Microphotographs of secondary trails of monophase (liquid) fluid inclusions within quartz crystals in the *La Piramide* Mn ores. C. Enlargement of A, which takes in evidence the secondary trails of fluid inclusion.

dinia from North to South. The climax of the volcanic activity occurred between 23 and 18 Ma, during the period of maximum extension of the Ligurian-Provençal basin (Lustrino et al., 2013).

The Sulcis Volcanic Province (SVP), located at the southwestern margin of Sardinia (Boni et al., 1990; Morra et al., 1994; Cioni et al., 2001), represents the last manifestations of the Oligo-Miocene igneous phase (Lustrino et al., 2013). This province includes the Sant'Antioco and San Pietro Islands and part of the Sulcis mainland. According to Morra et al. (1994), the SVP is characterized by two phases: an *Old Phase* (28.4–17.7 Ma) dominated by basaltic to intermediate lavas with subordinate pyroclastic products having calc-alcaline affinity and outcropping in the Sulcis mainland and in the Sant' Antioco Island; and a *Young Phase* (17.6–13.8 Ma), characterized by at least 11 main ignimbrite sheets ranging from trachytes to rhyolites in composition, with calc-alcaline to peralkaline affinity, that crop out in the Sulcis mainland and in Sant'Antioco and San Pietro Islands (Boni et al., 1990; Cioni et al., 2001; Mundula et al., 2009; Fig. 1A).

San Pietro is an island completely formed by volcanic terrains emplaced during the most recent portion of the *Young Phase* (Fig. 1A). Peralkaline, mainly comenditic, lava flows and ignimbrites extensively crop out in the northern part of the island, where some vents related to the effusive activity of this phase are also present (Araña et al., 1974; Garbarino et al., 1990). These peralkaline products are interlayered within the products of the calc-alkaline activity (Fig. 1B). All the volcanic products were subaerially emplaced within a time span of about 1 Ma starting from 15.8 Ma (Pioli and Rosi, 2005). Disseminated Mn-ores are present in some of the main units, being especially present in the peralkaline units (both lava flows and ignimbrites) or at the contact between these and the interlayered calc-alkaline units (Garbarino et al., 1990).

2.1. Mn mineralization of San Pietro Island

The Mn-ore deposits of San Pietro Island are part of the Sulcis-Iglesiente mining district. Based on available published data (Uras, 1965), the orebodies were roughly estimated to contain 400,000 tons of Mn ores, with a grade in the range of 5–40 wt% as Mn. The mineralization form irregular masses and vein swarms in the volcanic units. The largest deposit is, instead, a stratiform orebody of 4–8 m of thickness, intercalated with ochres and opal and quartz in a volcano-sedimentary environment (Guerin, 1973; Garbarino et al., 1990; Sinisi et al., 2012). Some of the Mn deposits of the San Pietro Island were considered economically exploitable in the past. This is the case of *Cala Fico*, *La Piramide*, *Capo Becco-Capo Rosso*, *Punta Nera-Le Lille* mines (Fig. 1A), where Mn ores were mined, with a fluctuating trend, throughout the last century until the 1970s when the mining activity definitively ended.

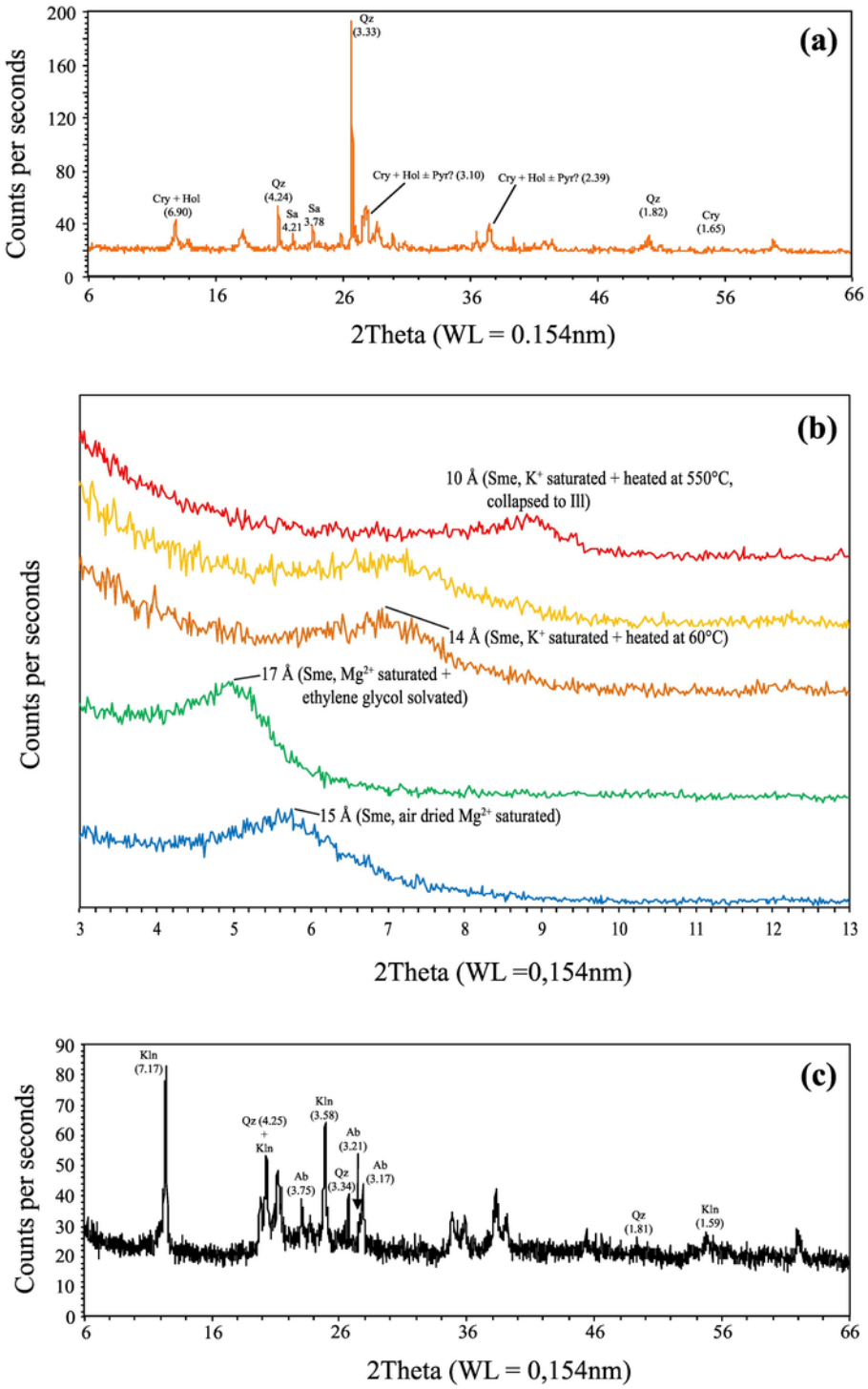

Fig. 6. Representative X-ray diffraction patterns of (a) San Pietro mineralization Mn oxides with peak positions provided for cryptomelane (Cry), hollandite (Hol) and possibly pyrolusite (Pyr). Quartz (Qz) and sanidine (Sa) peak positions are also indicated; (b) 001 reflection of smectite from the gangue of the Mn mineralization, on oriented mounts (blue: Mg^{2+} saturated in air dried state, green: Mg^{2+} saturated and ethylene glycol solvated, orange: K^{+} saturated and heated at 60 °C, yellow: K^{+} saturated and heated at 300 °C, red: K^{+} saturated and heated at 550 °C); (c) kaolinite (Kln) from *La Piramide* Mn mineralization. Quartz (Qz) and albite (Ab) peak positions are also indicated. (For interpretation of the references to colour in this figure legend, the reader is referred to the web version of this article.)

3. Analytical methods

Polished thin sections of the Mn-oxide veins and host rock were studied by means of reflected and transmitted light microscopy. The thin sections, as well as Mn-ore fragments, were carbon-coated and analyzed by SEM-BSEI (scanning electron microscope and back-scattered electrons imaging) and EDS (energy-dispersion spectroscopy) with a Philips XL30, equipped with an Edax Genesis microanalytical device (20 kV filament voltage, 10 mm working distance, up to 5000 magnifications) at the Department of Earth Sciences, University of Pisa, and by FE-SEM (field emission scanning electron microscope) and EDS with a

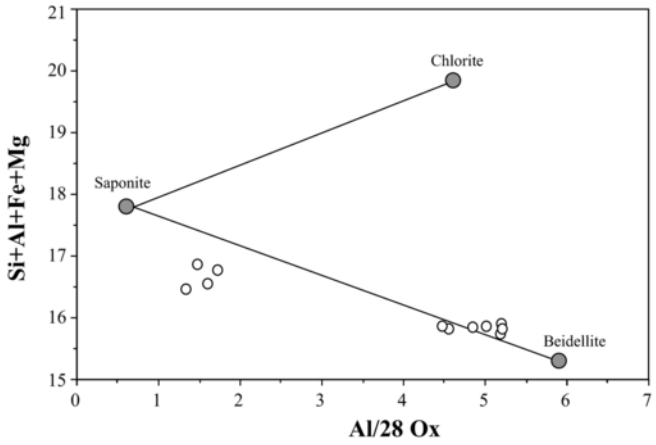

Fig. 7. Analyses of smectites associated with Mn ores plotted on the sum of the major non-interlayer cations (Si + Al + Fe + Mg) vs. Al diagram proposed by Schiffman and Fridleifsson (1991). All analyses recalculated on 28 oxygens basis.

FEI Quanta 450 equipped with a Bruker microanalytical system (20 kV filament voltage, 10 mm working distance, up to 60,000 magnifications) at the Centro Interdipartimentale di Scienza e Ingegneria dei Materiali, University of Pisa.

The samples from the Mn veins were crushed and the Mn ore manually separated from the host rock. Samples representative of the host rocks (lava and ignimbrites) were also crushed and visually cleaned of any Mn-ore impurities. In the case of ignimbrites, samples are representative of both the juvenile fraction (coarse juvenile clasts) and the bulk ignimbrite rock. The separated ore and host rock were finely powdered with agate ball mills.

The chemical composition of selected samples was determined by X-ray Fluorescence (XRF) on pressed powder pellets using an ARL 9400 XP+ sequential X-ray spectrometer under the instrumental conditions reported in Lezzerini et al. (2013). Within the range of the measured concentrations, the analytical uncertainties are <5% for all the components except for Na_2O, Al_2O_3, SiO_2, K_2O and MnO, which may occasionally attain <10% for very low concentrations (Lezzerini et al., 2013, 2014). The total amount of volatile components was determined as loss on ignition (LOI in 105–950 °C temperature range).

Trace-element analyses of veins and host rock were carried out with an inductively coupled plasma–mass spectrometer (ICP-MS; Perkin-Elmer NexION 300×) after sample digestion with aqua regia + HF at Department of Earth Sciences, University of Pisa. Accuracy is within ±5%. Analysis of REE concentrations was duplicated for two vein samples at ALS Chemex laboratories, by ICP-MS after lithium metaborate fusion.

Pb isotope ratios were determined at the Institute of Geosciences and Earth Resources (CNR) of Pisa using a Neptune MC-ICP-MS (Thermo Fisher Scientific Inc., Bremen, Germany). Lead was analyzed after HF-HNO_3 dissolution of 50–200 mg of sample, followed by standard ion-exchange chromatographic techniques. A thallium solution was added to both the sample and the standard to correct for instrumental mass fractionation. The dilute nitric acid solutions were injected into the mass spectrometer as aerosol through a quartz spray chamber. Only seven of the nine Faraday cup collectors of the Neptune MS were used in the measurement of Pb isotope ratios in static mode. Mercury was monitored for the correction of isobaric interference with ^{204}Pb, yet the signal of ^{202}Hg was four orders of magnitude smaller than that of ^{204}Pb in the measurement of sample solutions, so the effect of this interference was negligible as a matter of fact. Values used for mass bias fractionation corrections were $^{205}Tl/^{203}Tl = 2.388$. Measured values were compared with the international standard NBS981: $^{208}Pb/^{204}Pb = 36.7007$, $^{207}Pb/^{204}Pb = 15.4891$, $^{206}Pb/^{204}Pb = 16.9656$ (Todt et al., 1996). The reproducibility of the results of replicate analyses of the standard was 0.016–0.018% for the $^{206}Pb/^{204}Pb$, $^{207}Pb/^{204}Pb$, and $^{208}Pb/^{204}Pb$ ratios.

The qualitative mineralogical composition of bulk samples of both Mn ore and associated altered host rock was obtained by X-ray powder diffraction analysis (XRPD). The diffraction spectra were collected by an automatic diffractometer with Bragg-Brentano geometry, Bruker model D2 PHASER 2nd Generation equipped with a Lynxeye 1D detector and Ni-filtered CuKα radiation (λ = 1.5406 Å). Data were scanned within the angular range 5–65°2θ, with a step size of 0.02°2θ and a counting time of 0.3 s/step. The Bruker AXS DIFFRAC.EVA software was used for identifying the mineral phases.

XRPD analysis of the main phyllosilicates was carried out on one sample following the procedures described by Moore and Reynolds (1997). XRPD patterns were recorded using a Philips PW 1730 diffractometer with the following settings: CuK_α radiation obtained at 40 kV and 20 mA and graphite monocromator; slits: 1° divergence and scatter, 0.2 mm receiving; scan speed: 1°2θ/min; step size of 0.2°θ and counting time of 2 s per step. The clay mineral assemblage was studied on Mg^{2+} and K^+ saturated oriented mounts of the <2 μm fraction. The Mg^{2+} saturated specimens were measured in air-dried (AD) and glycolated (EG) states. K^+ saturated mounts were measured in air-dried conditions and after heating at 60, 300 and 550 °C. The basal reflections of clay minerals (including mixed-layer phases) were analyzed by the Brucker AXS DIFFRAC.EVA suite for phase analysis.

4. Results

4.1. Field reconnaissance

Samples representative of the Mn ore and associated volcanic host rocks were collected from the two abandoned mining sites of *La Piramide* (Il Macchione mine) and *Cala Fico*, located in the central and north-western area of the San Pietro Island, respectively (Fig. 1A).

At *La Piramide*, the main Mn mineralization is particularly concentrated at the contact between the Upper Comenditic Ignimbrite (UCI) and the overlying Monte Ulmus (MU) ignimbrite (above, Figs. 1B, 2A). Mn varnishes characterize the ignimbrite outcrop close to the mine entrances. The Mn ore consists of both individual centimeter-thickness veins and swarm veinlets (Fig. 2B). Nodules were also observed. The Mn-oxide mineralization is also found as disseminated spots in the host ignimbrite (O*celli* in Fig. 2C), showing a peculiar concentric texture. Locally, the pyroclastics are completely altered into a powdery whitish mass, suggesting an argillification process (Fig. 2D).

At *Cala Fico*, Mn oxide veins are widespread in a comenditic lava flow. The vein and veinlet swarms are parallel to the main fractures and either parallel or crosscutting the pervasive flow foliation of the rock (Fig. 2E). Locally, the ores occur also as patinae or crusts with a botryoidal structure. Nodules are not observed at this site.

4.2. Mineralogy and petrography

From a petrographic and mineralogical point of view, the UCI and MU ignimbrites show juvenile clasts with plurimillimetric quartz and alkali feldspar phenocrysts, and differ mainly for the lower abundance of quartz phenocrysts of the latter. Rare mineral phases typical of peralkaline products (aenigmatite, arfvedsonite, kaersutite, aegirine-augite) occur as microphenocrysts or in the groundmass. In the La Piramide outcrops, the original volcanic glass is strongly altered and shows spherulitic devitrification textures and zeolitization.

At *Cala Fico*, the porphyritic lava flow (phenocryst abundance of 25–30% by volume), has phenocrysts of quartz and alkali feldspar up to 5 mm, scarce kaersutite, aenigmatite and accessory zircon and fay-

Table 1
Geochemical analyses of Mn ores and of host rock at La Piramide and Cala Fico sites and of the unaltered juvenile fraction of UCI. Fe_2O_{3T}: all Fe as Fe_2O_3 wt%; L.O.I.: Loss on Ignition; bdl: below detection limit; –: not analyzed; Ce and Eu anomalies calculated with chondrite-normalized values (normalization values from McDonough and Sun, 1989). Pb isotope ratios: errors quoted are within run; the external reproducibility is between ±0.016 and ± 0.018% (2S.D.) for all ratios.

Sampling site	La Piramide	La Piramide	La Piramide	La Piramide	Cala Fico	La Piramide	La Piramide	Cala Fico	Punta Senoglio	Ventrisco
Description	Vein	Vein	Nodule	Ocelli	Vein	Host rock (bulk ignimbrite)	Host rock (bulk ignimbrite)	Host rock (lava)	UCI (unaltered juvenile fraction)	UCI (unaltered juvenile fraction)
Sample	QM-2v	QM-8v	QM-14v	QM-9o	QM-6v	QM-8	QM-9	SP-72	SP-66	SP-104
SiO_2 wt%	27.76	15.38	30.03	74.05	42.55	74.24	73.10	74.84	74.39	72.28
TiO_2	0.06	0.03	0.10	0.19	0.06	0.24	0.24	0.17	0.27	0.25
Al_2O_3	3.71	2.84	5.78	10.81	6.31	11.67	12.53	12.26	11.57	9.93
Fe_2O_{3T}	2.61	1.25	1.16	3.33	2.38	4.08	4.01	3.23	3.83	5.44
MnO	50.93	64.83	48.49	1.96	36.37	0.06	0.05	0.06	0.06	0.12
MgO	0.35	0.37	0.24	bdl	bdl	0.07	0.02	0.09	0.04	0,10
CaO	0.25	0.12	0.25	bdl	bdl	0.09	0.07	0.14	0.08	0.19
Na_2O	1.78	1.08	1.78	3.45	2.38	3.98	3.86	4.62	4.54	3.80
K_2O	3.61	2.87	4.14	4.38	4.54	4.44	4.39	4.59	4.52	4.03
P_2O_5	0.10	0.10	0.14	bdl	0.04	0.02	0.05	bdl	0.04	bdl
L.O.I.	8.84	11.13	7.89	1.83	5.37	1.11	1.68	0.99	0.66	3.85
Mn/Fe	21.78	57.88	46.65	0.66	17.05	0.02	0.01	0.02	0.02	0.02
$([K_2O] + [Na_2O])/[Al_2O_3]$	1.84	1.72	1.28	0.96	1.40	0.97	0.89	1.02	1.07	0.61
Li ppm	9.6	10.7	11.7	41	32.2	56	40	46	15.4	81
Be	62	55	53	6.9	43	7.1	5.6	7.2	6.3	12.6
Sc	2	3	2	7	4	6	6	5.1	5	5
V	15	12	15	6	7	1	1	<1	2	0.2
Cr	< 1	< 1	< 1	< 1	< 1	< 1	< 1	1.12	2	bdl
Co	7	11	3	< 1	70	< 1	< 1	<1	0.5	0.3
Ni	24	29	3	1	23	< 1	< 1	<1	1	1
Cu	2	3	2	1	92	< 1	< 1	–	–	–
Zn	627	639	513	117	1309	131	92	–	–	–
Ga	15.6	15.8	19.0	30.6	30.2	28.8	23.5	–	–	–
Rb	101	69	71	234	197	276	206	283	201	326
Sr	1652	2307	2666	21.5	552	9.6	5.9	3.07	15.7	5.6
Y	137	297	33.3	180	300	48	74	120	96	204
Zr	412	358	185	1539	278	1042	919	839	793	1695
Nb	52	32.5	55	167	111	131	98	112	105	192
Mo	9.8	1.30	19.9	15.8	126	0.78	0.43	0.68	2.2	9.4
Cs	1.38	5.1	4.5	0.74	3.29	0.93	0.62	4.2	2.96	11.3
Ba	8773	18,094	2995	779	2121	15.2	13.9	6.5	63	14
La	230	415	41	326	678	37	113	98	125	206
Ce	266	708	172	1053	2185	115	261	196	220	410
Pr	43	97	7.9	75	152	8.6	26.2	24.1	28.8	47
Nd	156	350	28.1	257	550	29.1	90	88.9	110	170
Sm	30.6	71	5.9	48	158	5.6	16.7	19.5	22.7	35
Eu	1.49	2.82	0.49	1.23	1.14	0.18	0.42	0.10	0.97	0,91
Gd	29.0	65	5.9	36	143	5.2	12.6	16.9	18.3	29.5
Tb	4.5	10.4	0.97	5.9	19.2	0.99	2.21	2.90	3.1	5.1
Dy	24.3	58	5.6	34	81	6.9	14.0	18.9	18.4	33
Ho	4.5	11.3	1.13	6.7	12.5	1.56	2.73	3.95	3.7	7.1
Er	11.3	30.0	3.08	19.2	26.0	5.1	8.1	11.2	9.9	19.7
Tm	1.50	4.0	0.43	2.95	2.94	0.90	1.29	1.80	1.57	3.1
Yb	8.6	22.3	2.55	19.1	15.6	6.3	8.5	10.7	9.2	17.9
Lu	1.23	3.25	0.38	2.76	2.02	1.09	1.28	1.54	1.32	2.65
Hf	9.9	7.9	3.9	29.0	7.8	23.8	20.2	22.8	20.1	41
Ta	2.58	1.79	1.93	8.8	4.9	8.8	7.1	8.0	7.1	13.6

Table 1 (*Continued*)

Sampling site	La Piramide	La Piramide	La Piramide	La Piramide	Cala Fico	La Piramide	La Piramide	Cala Fico	Punta Senoglio	Ventrisco
Description	Vein	Vein	Nodule	Ocelli	Vein	Host rock (bulk ignimbrite)	Host rock (bulk ignimbrite)	Host rock (lava)	UCI (unaltered juvenile fraction)	UCI (unaltered juvenile fraction)
Sample	QM-2v	QM-8v	QM-14v	QM-9o	QM-6v	QM-8	QM-9	SP-72	SP-66	SP-104
W	0.31	0.26	0.39	4.3	10.3	1.18	0.86	0.49	1.66	1.49
Pb	6.1	21.0	2.17	218	173	11.3	18.7	64	56	67
Th	12.6	11.8	3.3	55	21.3	34	34	35	23.8	50
U	11.0	22.1	5.8	6.2	20.4	2.33	2.62	5.2	6.4	13.3
ΣREE ppm	812	1847	276	1887	4026	224	558	495	573	987
Ce_N/Ce_N^*	0.56	0.77	2.04	1.47	1.48	1.40	1.05	0.89	0.86	0.97
Eu_N/Eu_N^*	0.17	0.14	0.28	0.10	0.03	0.11	0.10	0.02	0.12	0.10
$^{206}Pb/^{204}Pb$	18.9943 ± 0.0007	18.9271 ± 0.0004	–	–	18.7488 ± 0.0006	–	–	–		
$^{207}Pb/^{204}Pb$	15.6659 ± 0.0007	15.6685 ± 0.0003	–	–	15.6648 ± 0.0006	–	–	–		
$^{208}Pb/^{204}Pb$	38.9613 ± 0.0019	38.9284 ± 0.0008	–	–	38.7789 ± 0.0017	–	–	–		

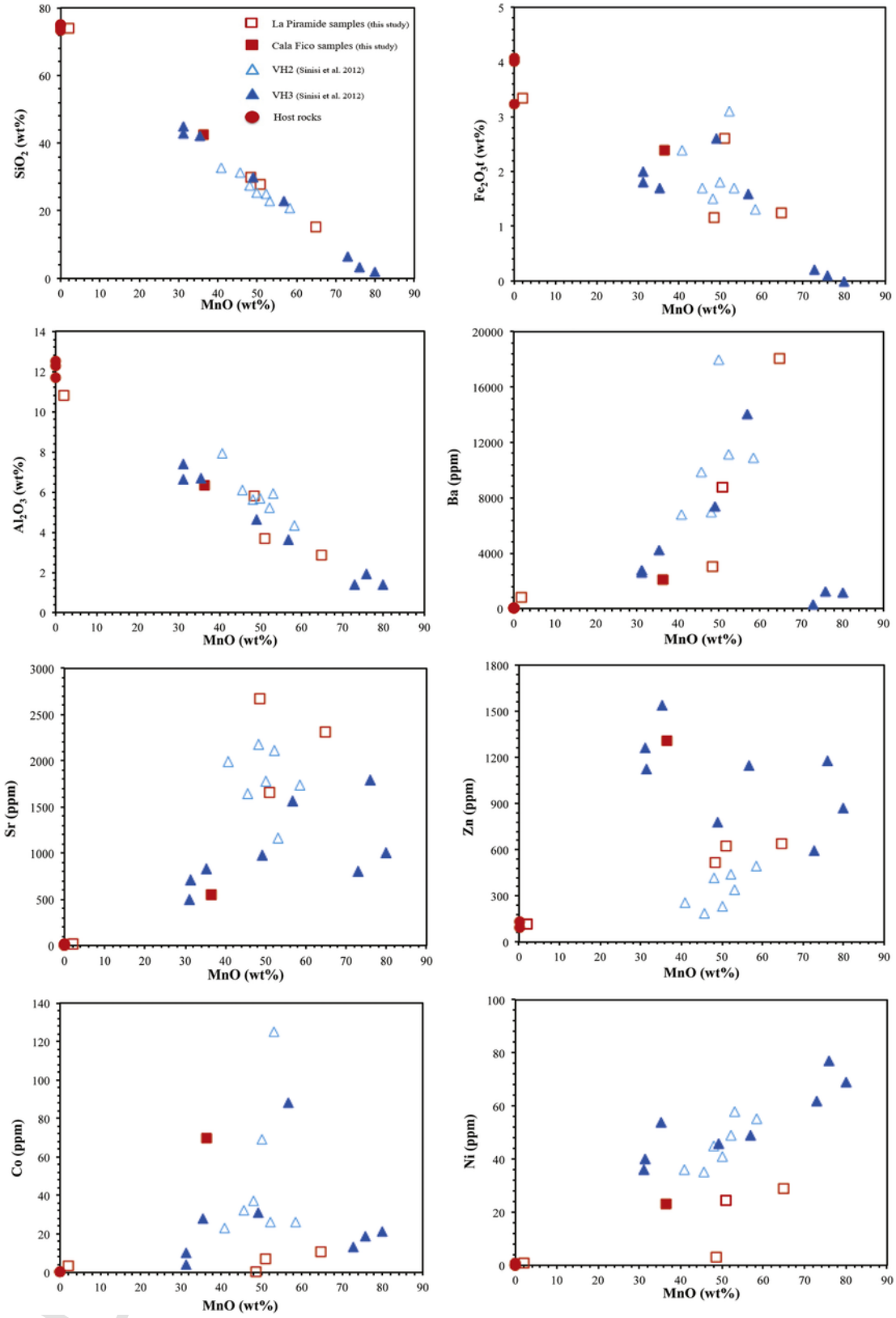

Fig. 8. Selected major and trace elements variation diagrams vs MnO (wt%) for Mn ore mineralization and host rock. Sinisi et al. (2012) data are reported for comparison (VH2 and VH3 samples from La Piramide and Cala Fico, respectively).

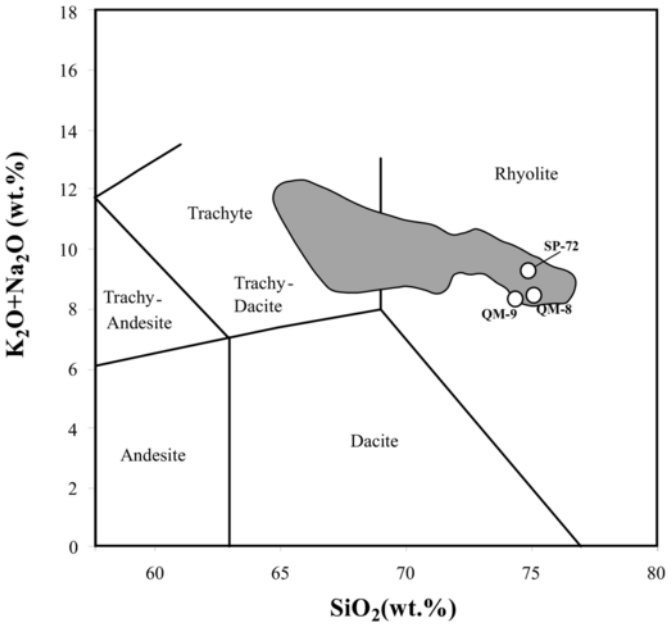

Fig. 9. Total alkali vs. SiO_2 (TAS) diagram of host rock samples of San Pietro Mn mineralization. Gray field represents the San Pietro volcanic rocks (from Lustrino et al., 2013 and Gisbert and Gimeno, 2016).

alite. The phenocrysts are hosted in a finely crystalline groundmass of quartz, feldspars and rare arfvedsonite.

The Mn mineralization in the two sites is epigenetic; the veins consist of fracture filling and/or of pervasive filling of the rock porosity by opaque Mn-bearing minerals. These show a variable crystallinity, passing from a cryptocrystalline matrix to well-crystallized phases. Pervasive filling is particularly evident in the highly porous ignimbritic lithologies at *La Piramide* (Fig. 3A, B). Open space filling is demonstrated by the observed colloform and botryoidal textures, indicating concentric overgrowths inward from vein walls (Fig. 3C), which in some cases leave incompletely filled cavities. In the ignimbrites, the Mn minerals fill the space between tabular crystals of secondary zeolites, overgrown on the volcanic glass (Fig. 3C). Similarly, in the peculiar disseminated mineralization (*Ocelli*) found at *La Piramide*, the Mn minerals form small concretions between the crystals of the host rock and line up the open spaces in the host rock matrix (Fig. 4A, B, C, D).

Large volcanic quartz and K-feldspar phenocrysts can be easily recognized within the ore (Fig. 4E). In some cases, the quartz crystals host secondary fluid inclusions trails. The inclusions are very small in size (< 5 μm) and monophase (Fig. 5).

Mn opaque minerals represent almost the totality of the mineralization. Under reflected light, different opaque minerals can be recognized in polished thin sections, based on different reflectivity (Fig. 3A, B). This is confirmed by BSE images (Fig. 4D). EDS analyses carried out on the Mn minerals with different reflectivity revealed a K-rich Mn oxide and a Ba-rich one (Table 2). The Ba- and K-rich Mn oxides are in some cases intimately intermixed (Fig. 4D). In agreement with the petrographic and EDS data, XRPD results suggest the presence of two different Mn minerals, cryptomelane and hollandite, respectively the K-rich and Ba-rich phases, although minor pyrolusite cannot be excluded (Fig. 6a).

Secondary REE-bearing minerals (apatite, monazite, cerianite) are scattered in the Mn mineralization. The close association of REE anomalies with the Mn mineralization is also indicated by the sparse occurrence of Ce peaks in EDS spectra (probably revealing unresolvable micron-sized Ce-oxides) in the brightest regions of BSE images of the Mn-rich matrix (Cala Fico mineralization, Fig. 4E, F).

Silica, barite and clays complete the ore paragenesis. Clays are dispersed with the pervasive mineralization and form the orange colored boundary visible at the margins of veins and nodules (Figs. 3D, 4G) both at La Piramide and Cala Fico. They are clearly associated to the Mn oxides, differently from other secondary minerals, probably zeolites (Fig. 4H), widespread in the ignimbrite matrix at La Piramide and pre-dating the Mn oxides. XRPD analyses of clay minerals on oriented mounts indicate smectite as the main mineralogical phase (Fig. 6b). Microanalytical EDS data (Table 2) are well in agreement with XRPD data and show a limited compositional variation among the analyzed smectites, which could be linked to the locally variable chemistry of the altered materials (Fig. 7).

At *La Piramide*, in correspondence of the Mn orebody, a pervasive clay alteration affects the pumice-bearing pyroclastics, resulting in a white-yellowish material with powdery appearance. XRPD analysis shows the occurrence of kaolinite (Fig. 6c).

4.3. Major and trace element geochemistry

Major and trace element composition of both the mineralization (vein and disseminated ores) and the host rock is reported in Table 1 and in the variation diagrams in Fig. 8. Data from Sinisi et al. (2012) for the same mining sites are also reported for comparison (VH2 and VH3 samples from La Piramide and Cala Fico, respectively). The rocks hosting the mineralization are rhyolitic (Fig. 9), peralkaline or close to peralkalinity (Table 1). The composition of the veins is enriched in MnO, Ba, Sr, Zr, U, Ni, Co and REE, but not in Fe_2O_3t, with respect to the rhyolite host rocks (Fig. 8). For several elements, the samples from *Cala Fico* and those from *La Piramide* sites plot in separate groups, showing distinct enrichment with respect to MnO content (Fig. 8). One sample of *La Piramide* mineralization (QM-9o) falls very close to the host rocks in all diagrams (Fig. 8). This sample represents the "Ocelli" Mn concretions and its chemical composition is strongly affected by contamination from the host rock.

4.3.1. REE geochemistry

Rare earth elements contents of mineralization and host rocks are shown in Table 1. The total REE content (ΣREE) of the mineralized samples displays a relatively wide range, from 276 to 4026 ppm, with an average value of 1740 ppm. These values are mostly well above those recorded in the associated host rocks (average ΣREE value of 426 ppm with a maximum value of 558 ppm). Remarkably, also the QM-9o sample ("Ocelli"), which shows clear evidences of strong contamination by the host rock, results enriched in REE with respect to the host rock.

The chondrite-normalized distribution patterns of REE in the mineralized samples are characterized by a significant fractionation between the LREE and the HREE, which is higher than in the host rocks (Fig. 10). La/Lu ratios in Mn ore are indeed between 107 and 336 with an average value of 189, whereas they vary from 34 to 88, with an average value of 62, in the host rocks.

In the mineralized samples, the values of $(Ce/Ce^*)_{CN}$ vary from 0.56 to 2.04, thus showing either a positive (QM-6v, QM-14v) or negative (QM-2v, QM-8v) Ce anomaly (Fig. 10, Table 1). The Eu anomaly, expressed as $(Eu/Eu^*)_{CN}$, is negative in all the analyzed samples. It varies from 0.02 to 0.28, with an average value of 0.15, in the mineralized samples. These values are slightly higher than those shown by the host rocks (between 0.02 and 0.11, with an average value of 0.08).

4.4. Pb isotope geochemistry

The Pb isotope ratios of three samples of Mn-oxide veins, one from *Cala Fico* and two from *La Piramide*, are reported in Table 1. The manganese mineralization of *Cala Fico* has $^{206}Pb/^{204}Pb = 18.749$,

Table 2
EDS analysis of Mn ores and alteration mineral in representative samples of La Piramide and Cala Fico sites. Smectite formulas calculated based on 22 oxygens. Cry = Cryptomelane; Hol = Hollandite; Mnz = Monazite; Sm = Smectite; –: not analyzed.

Sampling site	La Piramide	La Piramide	La Piramide	La Piramide	La Piramide	Cala Fico	La Piramide	La Piramide
Sample	QM-8v	QM-8v	QM-8v	QM-2v	QM-2v	QM-6v	QM-8v	QM-2v
Phase	Cry	Cry	Cry-Hol	Hol	Cry-Hol	Mn + Ce	Mnz(Ce)	Mnz(La)
SiO_2	0.61	0.30	4.58	19.34	0.44	10.60	3.09	–
Al_2O_3	0.33	–	2.71	5.53	0.64	1.91	–	0.44
FeO_{TOT}	0.19	0.20	2.65	1.41	0.82	0.34	1.02	–
MnO	91.27	92.24	80.75	61.28	90.8	41.66	4.31	19.99
MgO	0.48	0.56	0.74	1.03	0.38	0.99	–	0.26
CaO	0.27	0.13	0.36	0.41	–	1.08	–	6.08
Na_2O	0.79	0.61	0.62	2.62	0.33	–	1	–
K_2O	5.2	5.45	3.9	2.60	3.27	1.21	0.65	1.03
ClO	–	–	–	–	–	1.78	–	–
SO_3	–	–	–	–	–	–	–	0.26
BaO	0.86	0.39	3.68	5.78	3.31	–	0.66	–
ZnO	–	0.12	–	–	–	–	–	–
P_2O_5	–	–	–	–	–	2.03	30.51	32.04
La_2O_3	–	–	–	–	–	–	22.28	23.96
Ce_2O_3	–	–	–	–	–	38.25	29.84	0.49
Nd_2O_3	–	–	–	–	–	–	6.63	15.45
Tot.	100	100	99.99	100	99.99	99.85	99.99	100

Sampling site	La Piramide	La Piramide	La Piramide	La Piramide	La Piramide	La Piramide
Sample	QM-8v	QM-8v	QM-8v	QM-2v	QM-2v	QM-2v
Phase	Sm	Sm	Sm	Sm	Sm	Sm
SiO_2	55.91	53.82	55.02	55.64	55.60	55.30
TiO_2	–	–	0.71	0.93	0.92	0.68
Al_2O_3	7.60	6.92	6.34	27.92	27.84	27.47
FeO_{TOT}	30.51	34.47	27.75	10.96	10.64	10.78
MnO	0.48	0.35	0.74	1.03	0.76	1.20
MgO	1.56	1.44	4.66	1.46	1.52	1.23
CaO	2.28	2.44	2.80	1.32	1.44	1.62
Na_2O	0.30	0.12	1.07	0.27	0.45	0.25
K_2O	1.36	0.44	0.91	0.77	0.83	1.47
Tot.	100	100	100	100	100	100
Si	7.83	7.68	7.67	6.96	6.94	6.95
Ti	–	–	0.07	0.09	0.09	0.06
Al	1.25	1.16	1.04	4.07	4.10	4.07
Fe^2	3.57	4.11	3.24	1.15	1.11	1.13
Mn	0.06	0.04	0.09	0.11	0.08	0.13
Mg	0.33	0.31	0.97	0.27	0.28	0.23
Ca	0.34	0.37	0.42	0.18	0.19	0.22
Na	0.08	0.03	0.29	0.07	0.11	0.06
K	0.24	0.08	0.16	0.12	0.13	0.24

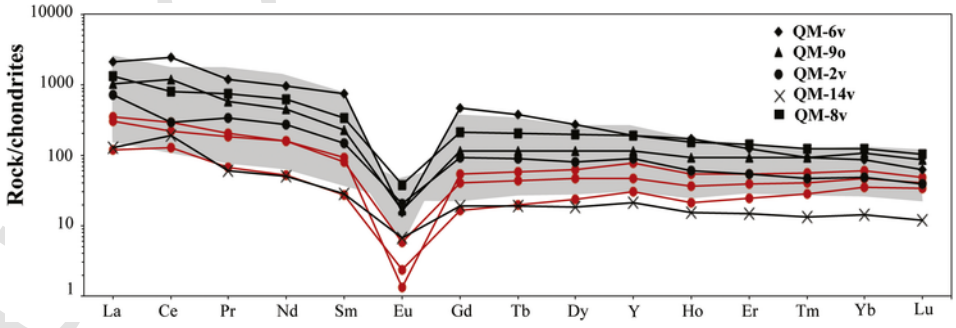

Fig. 10. Chondrite-normalized REE patterns of San Pietro Island Mn-ore (black) and host rock (red) samples. Chondrite normalizing values from McDonough and Sun (1989). REE data on San Pietro Mn ore from Sinisi et al. (2012) are reported for comparison (gray area). (For interpretation of the references to colour in this figure legend, the reader is referred to the web version of this article.)

$^{207}Pb/^{204}Pb = 15.665$ and $^{208}Pb/^{204}Pb = 38.779$. The two samples of the mineralization of *La Piramide* differ from the one of *Cala Fico*, having $^{206}Pb/^{204}Pb$, $^{207}Pb/^{204}Pb$ and $^{208}Pb/^{204}Pb$ of 18.927–18.994, 15.666–15.668 and 38.928–38.961, respectively (Table 1). In Fig. 11, the Pb data of the analyzed veins are displayed along with those of both the sulfide ores from the Iglesiente-Sulcis area (Boni and Koeppel,

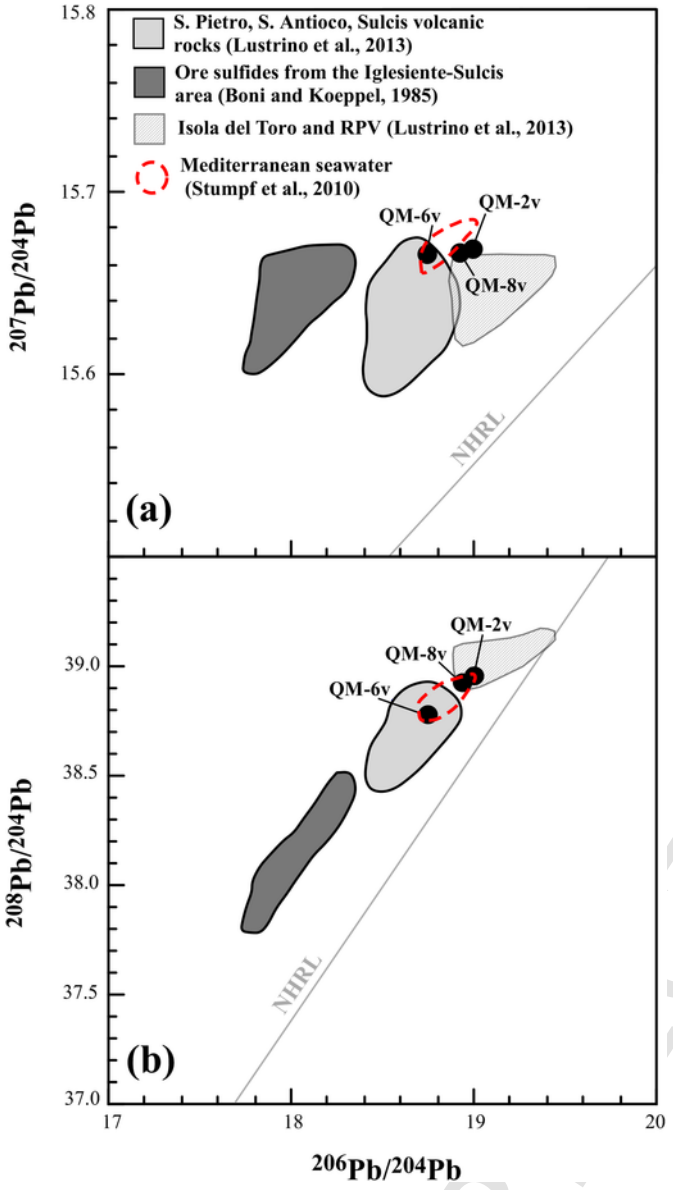

Fig. 11. (a) $^{207}Pb/^{204}Pb$ and (b) $^{208}Pb/^{204}Pb$ vs. $^{206}Pb/^{204}Pb$ for San Pietro Mn mineralization compared with the Pb isotope data of San Pietro, Sant'Antioco, Sulcis and Isola del Toro and RPV (Radiogenic Pb Volcanics, see Lustrino et al., 2000) volcanic rocks (Lustrino et al., 2013) and ore sulfides from the Sulcis Iglesiente area (Boni and Koeppel, 1985). Mediterranean seawater field (Stumpf et al., 2010) is also reported for comparison. NHRL: Northern Hemisphere Reference Line (Hart, 1984).

1985), and the Cenozoic volcanic rocks of Sardinia (Lustrino et al., 2013). Here, a separation between *Cala Fico* and *La Piramide* deposits can be seen: the sample from *Cala Fico* falls in the field of the Sulcis magmatic rocks, whereas the samples from *La Piramide*, having more radiogenic Pb isotope ratios, do not overlap to the Sulcis magmatic rocks and approach the field of some Plio-Pleistocene volcanic rocks outcropping in southern Sardinia (called RPV, radiogenic Pb volcanic rocks, by Lustrino et al., 2000) and marking the passage from the Tertiary orogenic to the Plio-Pleistocene anorogenic volcanism of Sardinia (Lustrino et al., 2007).

5. Discussion

5.1. Insights into the composition and temperature of the mineralizing fluids

Some insights concerning temperature, composition and pH conditions of the fluids responsible for Mn ore formation can be deduced from the mineralogical assemblage of alteration associated to the mineralization (Browne, 1978; Pirajno, 1992 and references therein).

The secondary mineralogical assemblage of host rocks is dominated by phyllosilicates (dioctahedral smectites and, locally, kaolinite) and zeolites. Petrographic evidence indicates that zeolites precede Mn minerals, probably representing post-depositional alteration of the ignimbrite glassy matrix. The mineralogical alteration paragenesis associated to Mn oxides, mainly characterized by smectites with minor kaolinite, identifies an argillic facies and reflects weak acidic conditions (pH indicatively of 5) and relatively low temperature (< 150 °C) of formation. The low temperature is also confirmed by the occurrence of secondary fluid inclusion assemblages, formed by very small monophase inclusions (< 5 μm), which suggest temperature below 100 °C.

Inferences on the composition of the mineralizing fluids are obtained by comparing the chemical compositions of the ores and host rock (Fig. 12). The comparison shows that, in addition to Mn, the ores are remarkably enriched in Ba, REE and Y (REY) and Sr and are slightly enriched in Co, Ni, Cu and Zn. This suggests that these elements were introduced by the mineralizing fluids.

5.2. Geochemical constraints on the genetic classification of ores and origin of fluids

Several works concerning the genesis of Mn ore deposits have been carried out (Aplin and Cronan, 1985; Halbach et al., 1988; Roy, 1992, 1997; Hein et al., 1997; Hein and Koschinsky, 2013; Josso et al., 2017). Mn oxides are deposited in terrestrial and marine environments by hydrogenetic, supergene and hydrothermal processes (Nicholson, 1992; Roy, 1992). In the marine environment these deposits are generally classified into three main categories corresponding to different formation mechanisms (Bonatti et al., 1972; Roy, 1992; Nicholson, 1992; Hein et al., 1997; Bau et al., 2014; Schmidt et al., 2014): hydrogenetic, deriving from precipitation from ambient seawater; diagenetic, deriving from cold porewater below the seafloor during diagenesis; hydrothermal, deriving from precipitation occurred in the vicinity of hydrothermal vents at or below the seafloor. Consequently, the Mn ores forming the mineralization may have different mineralogical components and geochemical compositions. Geochemical features, particularly the contents of transition metals (Mn, Fe, Cu, Co, Ni, Zn, Pb) and As, and contents, ratios and distribution patterns of REY, are the main indicators used to identify different genetic types of Mn mineralization. Accordingly, several classification diagrams were proposed in the literature (Bonatti et al., 1972; Nicholson, 1992; Bau et al., 2014; Josso et al., 2017).

In the triangular discrimination diagram (Fig. 13a) recently proposed by Josso et al. (2017), the San Pietro volcanic-hosted Mn ore data (this work and Sinisi et al., 2012), plot very close to the (Fe + Mn)/4–100*(Zr + Ce + Y) side of the diagram, describing a trend between the hydrogenetic and hydrothermal end-members. Plotting the data in the discrimination diagrams based on REY, proposed by Bau et al. (2014), these show a trend between the hydrogenetic and hydrothermal fields in the Ce_{SN}/Ce_{SN*} vs Y_{SN}/Ho_{SN} (Fig. 13b), similarly to the previous diagram. In the Ce_{SN}/Ce_{SN*} vs Nd graph (Fig. 13c), on the other hand, part of the San Pietro samples plots in the hydrogenetic field, while some, although showing high Nd in agreement with hydrogenetic features, display negative Ce anomalies. Bau et al. (2014) interpreted this behavior, for marine Mn ores, as due to a mixed hydrother-

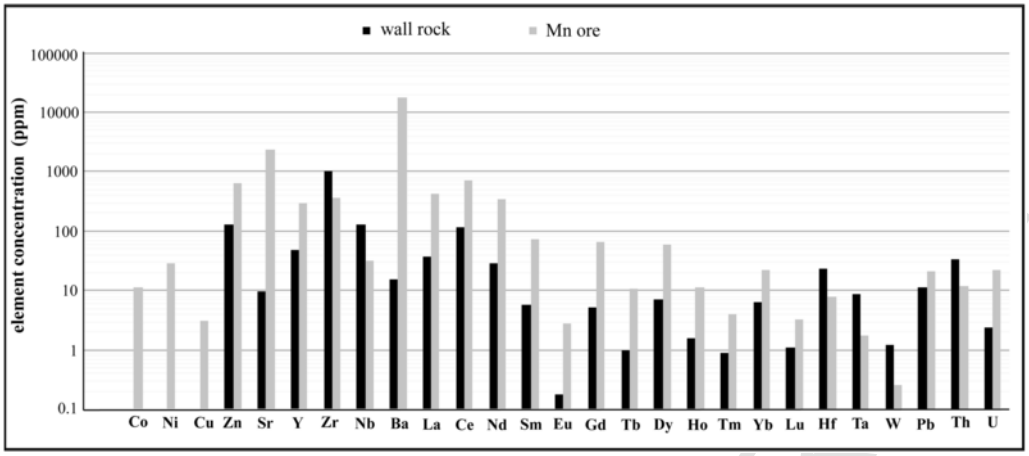

Fig. 12. Histogram showing the comparison of trace element concentration between host rock and Mn ore.

mal-hydrogenetic mechanism, which limited the Ce preferential accumulation by oxidative scavenging from seawater. Combined hydrothermal-hydrogenetic processes have been also proposed for other different types of Mn ore deposits to explain intermediate geochemical features (e.g. Conly et al., 2011; Xiao et al., 2017). Based on the above, we propose that two mechanisms – hydrothermal and hydrogenetic – have been active to give the geochemical characteristics of San Pietro ores. The occurrence of a hydrothermal component, enriched in H_2S, was possibly responsible for the weak acidic (pH around 5) conditions of the mineralizing fluids, as suggested by alteration mineralogy (see Section 5.1).

Regarding the Pb isotopes, the signatures of both *Cala Fico* and *La Piramide* mineralization are clearly distinguishable from those of the sulfide ores from the Iglesiente-Sulcis area, whereas they approach those of the Sardinian Cenozoic volcanic rocks (Fig. 11). However, samples from different veins show a substantial spread in their Pb isotope ratios. Such a spread suggests a contribution of multiple sources of fluids in the genesis of the San Pietro mineralizations. In particular, the *Cala Fico* sample (QM-6v) falls in the field of San Pietro-Sant'Antioco-Sulcis volcanic rocks. Thus, an interaction with hydrothermal fluids circulating in the surrounding volcanic rocks can be inferred in the formation of *Cala Fico* Mn mineralization. The *La Piramide* samples (QM-2v, QM-8v), instead, plot either inside (Fig. 11b) or close (Fig. 11a) to the field of Radiogenic Pb Volcanics (RPV, Lustrino et al., 2000), some of which were emplaced in SW Sardinia not far from San Pietro Island at 11.8 Ma (Isola del Toro). This similarity could indicate the RPV as a plausible additional source of hydrothermal fluids. On the other hand, the Pb isotope ratios of seawater from the Mediterranean Sea at various depths (Fig. 11) define a field that overlaps almost completely the trend delineated by the San Pietro Mn mineralization. Hence, a contribution from seawater can also be envisaged based on the presented data.

The above interpretation differs from the ore-forming model proposed by Sinisi et al. (2012), in which they envisaged the San Pietro volcanic-hosted ores originated from the mixing of magmatic fluids and meteoric waters. Indeed, the relatively low temperature of formation of these Mn mineralizations, estimated by the mineralogical alteration assemblage and the occurrence of monophase secondary fluid inclusions (see Section 5.1 paragraph), would rule out the involvement of high-temperature magmatic fluids in the genesis of these Mn ores. We must furthermore take into account that, differently from what reported in other Mn ore mineralization on volcanic islands (Liakopoulos et al., 2001; Kilias et al., 2001; Naden et al., 2005; Lykakis and Kilias, 2010; Papavassiliou et al., 2017), no evidence of epithermal mineralization occurs at San Pietro. This indicates that a high temperature hydrothermal (and/or magmatic-hydrothermal) system was not involved in the Mn metallogenesis on the island.

5.3. Mn and REE sources

With the aim of evaluating the absolute mobility of the elements in the host rocks affected by low temperature hydrothermal alteration, and their possible contribution to the mineralization (particularly in terms of Mn and REE contents), we took into account the variation of mass induced by alteration. For this reason, the data were processed using the isocon diagram method (Grant, 1986), which represents a graphical solution of the Gresens (1967) equation (see Appendix).

The isocon diagram (Fig. 14a) shows that Mn substantially behaves as an immobile element and does not undergo any depletion during hydrothermal alteration of San Pietro volcanics. This indicates that volcanic host rocks cannot be viewed as a possible source of Mn for the mineralization on the island. Mn may conversely derive from remobilization of Mn oxides sequestered in shelf and slope sediments and/or by leaching of the older Cenozoic volcanic rocks that form the basement of the island and surroundings. Both sources, as a matter of fact, are in agreement with Pb isotope data (Fig. 11). A possible Mn contribution also from hydrothermal vents into the upwelling seawater masses cannot be excluded.

A different behavior is shown by the REE, which result strongly depleted in the hydrothermally altered host rocks (Fig. 14a, b). In this case, volcanic host rock could represent a possible source of the REE found in the mineralization. The similarity between the REE patterns of the Mn mineralization and of the host rocks (Fig. 10) would support this hypothesis. The control exerted by the host rocks over the Mn mineralization, as evidenced by the REE pattern, could be related to the hydrothermal alteration of apatite and monazite, which represent an important storage for REE in magmatic environment, with subsequent leaching of these elements and their re-precipitation within the disseminated hydrothermal cerianite and monazite crystals found in the mineralization (Mongelli et al., 2013).

The higher LREE/HREE ratios of the Mn ores (La/Lu = 107–336; Table 1) with respect to the host rocks (La/Lu = 34–88; Table 1) are in agreement with the role played by re-precipitation of hydrothermal LREE-bearing apatite, monazite and cerianite observed in the studied samples (Fig. 4F). Furthermore, we must take into account that the REE partitioning between Mn marine ores of hydrogenetic origin and seawater tends to increase the LREE/HREE ratio and Mn oxhydroxide colloidal particles preferentially absorb LREE. Consequently, the influence of a hydrogenetic component (Fig. 13) could have further favored the increase of the LREE/HREE ratio in the Mn mineralization with respect to the host rocks.

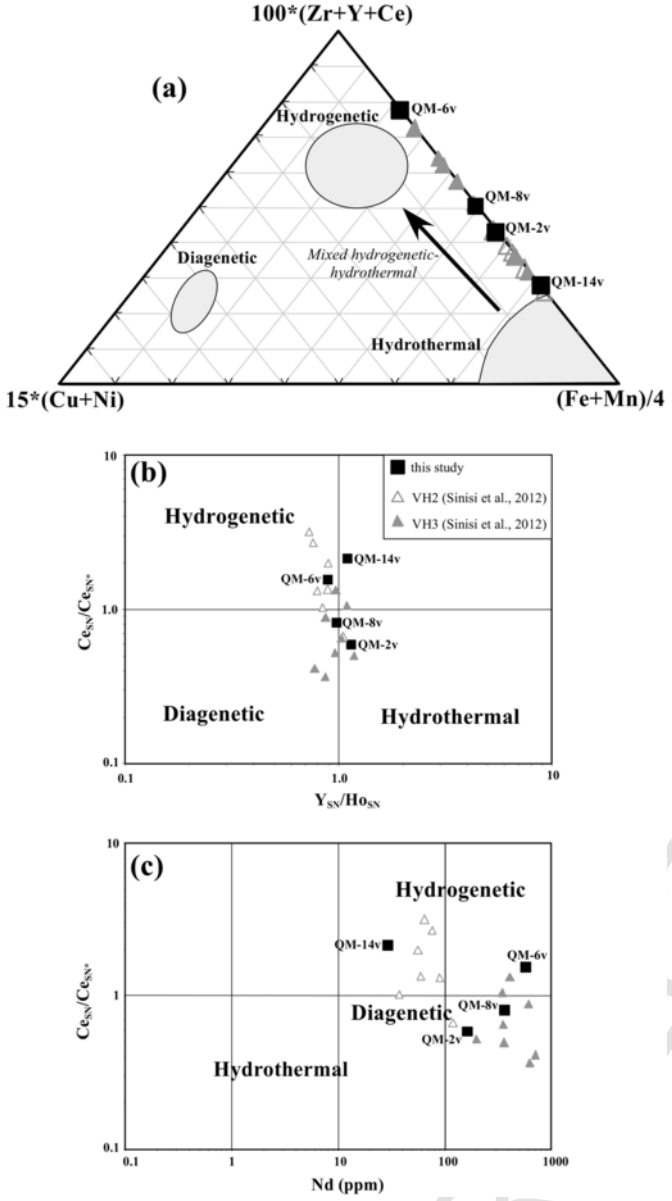

Fig. 13. (a) Plot of San Pietro Island Mn ore composition on ternary discriminative graph for genetic classification of Fe-Mn deposits after Josso et al. (2017). (b) Ce_{SN}/Ce_{SN}^* vs. Y_{SN}/Ho_{SN} and (c) Ce_{SN}/Ce_{SN}^* vs. Nd concentration diagrams of San Pietro Island Mn ores, based on Bau et al. (2014). Subscript "SN"; shale is Post-Archean Australian Shale, PAAS, of McLennan (1989). Sinisi et al. (2012) data are reported for comparison (VH2 and VH3 samples from La Piramide and Cala Fico, respectively).

5.4. Mn metallogenesis

Mineralogical and geochemical data help constraining the conditions of formation of the Mn deposits on San Pietro Island and allow proposing a metallogenetic model. The Ce behavior in the mineralization provides evidence about the oxidation state of the fluid, as Ce is a redox-sensitive REE (Holster, 1997). In oxic environment, soluble Ce^{3+} is oxidized into insoluble Ce^{4+} as CeO_2 and tends to be rapidly removed from fluid via scavenging by Mn and/or Fe oxyhydroxides or by organic matter in suspension, thus producing a strong negative Ce anomaly in the oxidized waters (Holster, 1997; Pourret et al., 2008). Consequently, Mn mineralizations of hydrogenetic origin are characterized by prominent positive Ce anomalies (Bau et al., 1996, 2014; Pattan et al., 2005; Surya Prakash et al., 2012). The Ce anomaly shown by Mn mineralization of San Pietro Island suggests a shallow, oxidizing environment of deposition. This is in agreement with the absence of Mn carbonates in the ore mineralogy (Fig. 15). The positive Ce anomaly displayed by some samples may also suggest a derivation of Mn from remobilization of hydrogenetic Mn oxides possibly sequestered in shelf and slope sediments (Fig. 16). The reconstruction of eustatic changes of the seawater level in Sardinia area evidenced several episodes of sea level rise during Miocene (Cherchi and Montadert, 1982). As a consequence, we may hypothesize that the sea level rise allowed a later seawater influx within ignimbritic units at San Pietro, after their sub-aerial emplacement, and the development of the shallow water oxidizing conditions that led the deposition of Mn ores.

Assuming an initial pH around 5, caused by the ascent of hydrothermal fluids enriched in H_2S (see Sections 5.1, 5.2 paragraphs), we propose that the precipitation of Mn ore could have been induced by the neutralization of pH of the fluids as a results of water-rock interaction processes (Fig. 15), i.e. hydrolysis reactions. Indeed, in hydrolysis, H^+ is typically consumed by the reaction with silicate minerals, provoking the conversion of anhydrous silicates to hydrous ones (i.e. clay minerals, mainly depending on the temperature) and the release of metal ions into the solution (Pirajno, 1992). This in turn causes the pH increase of the fluid. The occurrence of smectites in the alteration paragenesis associated to our Mn mineralization well agrees with the occurrence of water/rock interaction processes mainly driven by hydrolysis reactions (Fig. 15).

6. Conclusions

Geochemical, mineralogical, and isotopic data allowed proposing a metallogenesis model for the San Pietro Island Mn ore deposits.

Based on the geochemical relationships characterizing the concentrations of REE and transition metals in different genetic models of Mn oxide deposits, we suggest a mixed hydrothermal-hydrogenetic component in the fluids that formed San Pietro Island Mn deposits (Fig. 16). Mn-bearing fluids were originated from the remobilization of Mn oxides sequestered in shelf and slope sediments – providing the hydrogenetic signature – and/or by leaching of the older Cenozoic volcanic rocks. Then these fluids entered the hydrothermal convection, possibly linked to the general thermal anomaly that interested the area from 15 to 12 My (San Pietro, Sant'Antioco, Isola del Toro volcanic activity). The mineralizing fluids, probably dominated by seawater and made acidic by the input of H_2S of hydrothermal origin, were characterized by oxidizing conditions and relatively low temperatures (<100–$120\,^{\circ}C$). The Mn ore deposition occurred in a shallow water environment, as a result of the pH neutralization induced by water-rock interaction processes. The Pb isotopes, although based on a limited number of samples, also agree with the above presented model, as the signatures of the San Pietro veins seem to define a possible multi-component mixing, with contributions from (i) country rocks of San Pietro, (ii) a component similar to the southern Sardinian RPV (e. g. Isola del Toro), and (iii) seawater. Further isotope investigation could help to better define the mode of interaction and the involved components.

Acknowledgements

The authors warmly thank M. D'Orazio for help in ICP-MS analysis, G. Ruggieri for help and suggestions on fluid inclusion data and F. Colarieti for assistance during analytical work. We are grateful to S. Agostini for his assistance during the preparation and measurements of the Pb isotopes. This study was funded by University of Pisa "Fondi d'Ateneo" (MIUR) to AG. We greatly appreciated comments and suggestions by two anonymous reviewers.

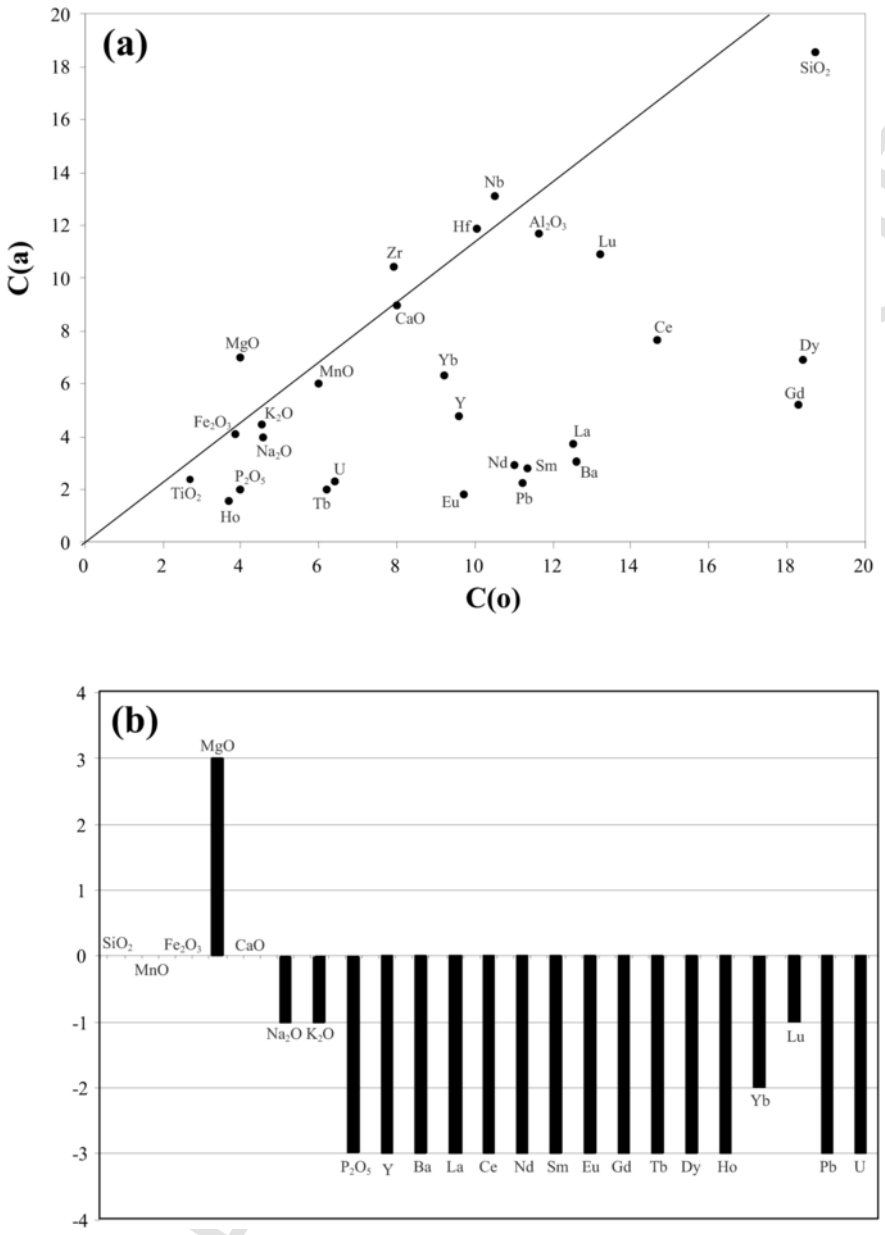

Fig. 14. (a), (b) Isocon diagram (upper) and histogram showing percentage of gains and losses (bottom) of selected elements during hydrothermal alteration of Mn mineralization host rock, as calculated from isocon diagram method (see Appendix). Variation of +4 to +1 = a gain of >100%, 50 to 100%, 25 to 50% and 10 to 25%, respectively. 0 = immobile elements (variation in the range + 10 and − 10%). Values of −1 to −4 = losses of 10 to 25%, 25 to 50%, 50 to 90%, >90%, respectively.

Appendix A

The isocon method involves plotting elemental abundances of the altered rocks (C^a) against those of the fresh equivalent (C^o) and determining the position of the isocon (straight line that joins the points of equal geochemical concentration) by fitting a series of elements assumed to be immobile. The slope of the isocon (M^o/M^a) is the fundamental ratio of equivalent masses before and after alteration (Grant, 1986). In this work, we considered Al, Ti, Zr and Hf as immobile elements. The isocon straight line can be described by the equation

$$C^a = \left(M^o/M^a\right) \cdot C^o \quad (1)$$

where C^a = concentration of an immobile element in the altered rock, C^o = concentration of an immobile element in the fresh rock, M^a = mass of the altered rock, M^o = mass of the fresh rock. The geometry of the diagram is such that the elements below the isocon are depleted whereas those above are enriched. It is possible to evaluate enrichment or depletion of the various elements by using the following equation:

$$\left(\Delta C_i/C_i\right) \cdot 100 = \left(M^a/M^o\right) \cdot \left(C_i{}^a/C_i{}^o\right) - 1 \quad (2)$$

where $(\Delta C_i/C_i)\cdot 100$ is the percentage variation of the i^{th} element in the altered rock compared with the fresh rock (Grant, 1986).

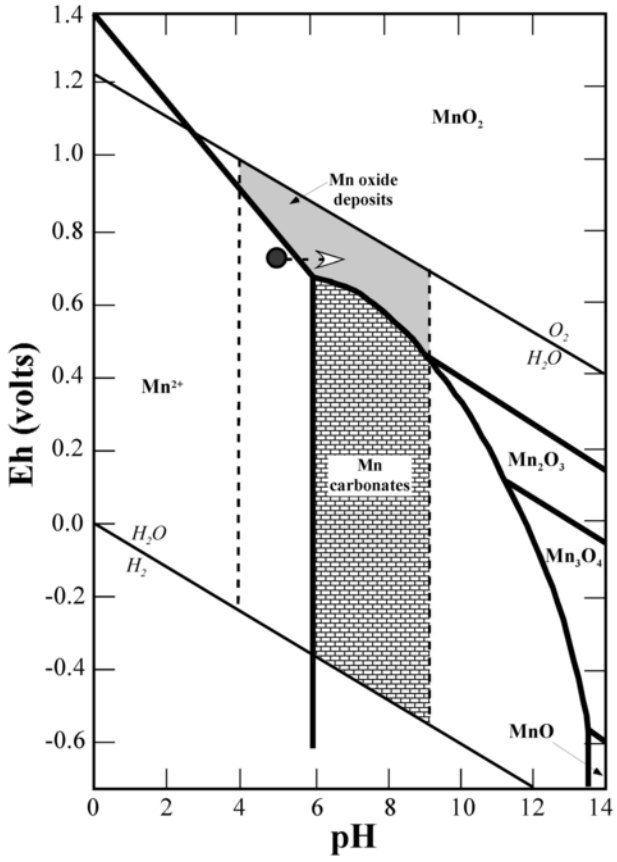

Fig. 15. Eh-pH diagram showing the stability of Mn oxide and Mn carbonates deposits in natural water (after Roy, 2006, modified). The diagram is built assuming Mn^{2+}; total carbonates and sulfur concentrations of 10^{-6}, 1 and 10^{-6} M respectively, according to Roy (2006). The dashed lines enclose the boundary of natural water. The dark gray circle represents the indicative Eh-pH conditions of the ore forming fluid at San Pietro Island; the dashed arrow indicates the shift of the Eh-pH conditions that led to Mn ore precipitation (see text for details).

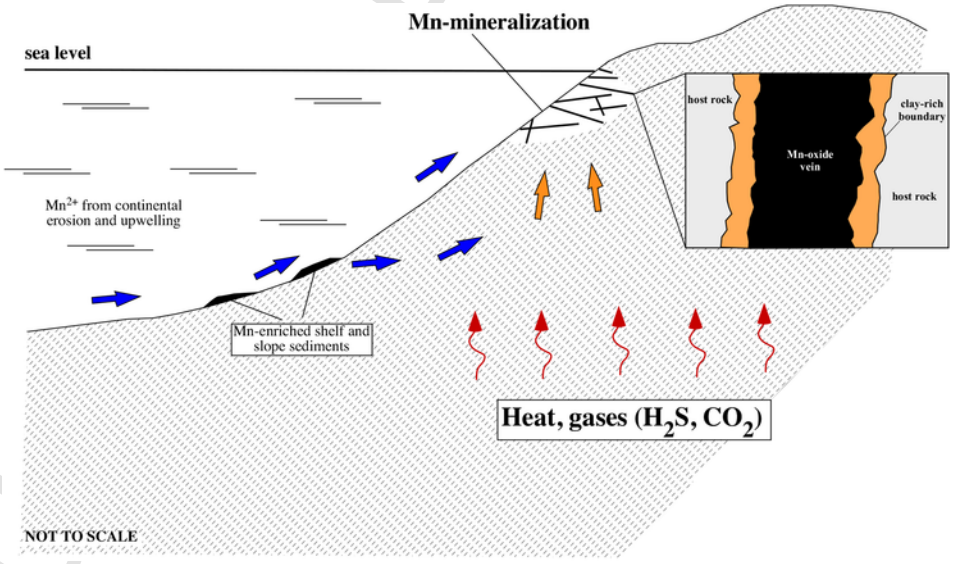

Fig. 16. Schematic sketch of the metallogenic model of San Pietro Island Mn mineralization. The insert represents the scheme of a typical Mn-oxide vein within the ignimbrite host rock, bounded by clay-rich rims produced as a consequence of water/rock interaction processes (see text for explanation).

References

Aplin, A.C., Cronan, D.S., 1985. Ferromanganese oxide deposits from the central Pacific Ocean, II. Nodules and associated sediments. Geochim. Cosmochim. Acta 49, 437–451.

Bau, M., Koschinsky, A., Dulski, P., Hein, J.R., 1996. Comparison of the partitioning behaviours of yttrium, rare earth elements, and titanium between hydrogenetic marine ferromanganese crusts and seawater. Geochim. Cosmochim. Acta 60, 1709–1725.

Bau, M., Schmidt, K., Koschinsky, A., Hein, J.R., Usui, A., 2014. Discriminating between different genetic types of marine ferro-manganese crusts and nodules based on rare earth elements and yttrium. Chem. Geol. 381, 1–9.

Bonatti, E., Kraemer, T., Rydell, H., 1972. Classification and genesis of submarine iron-manganese deposits. In: Horn, D. (Ed.), Ferromanganese Deposits on the Ocean Floor. Natl. Sci. Found, Washington, pp. 149–165.

Boni, M., Koeppel, V., 1985. Ore-lead isotope pattern from the Iglesiente-Sulcis area (SW Sardinia) and the problem of remobilization of metals. Mineral. Deposita 20, 185–193.

Boni, M., Del Vecchio, L., Lirer, L., 1990. Considerazioni sul vulcanismo miocenico della Sardegna sud-occidentale. Atti 75° Congresso Società Geologica Italiana, Milano 1990. Mem. Soc. Geol. Ital. 45, 989–1000.

Boni, M., Iannace, A., Balassone, G., 1996. Base Metal Ores in the Lower Palaeozoic of SouthWestern Sardinia. Econ. Geol. 75th Anniversary Volume, Spec. Publ. 4. 18–28.

Botta, P., Salvadori, I., Garbarino, C., Orrù, P.E., Rizzo, R., Cioni, R., Patta, E.D., Puliga, G., Deina, G., Coltorti, M., Gattaceca, J., Mundula, F., 2015. Carta Geologica d'Italia: Isola di San Pietro, Foglio 563, 1:50.000. I.G.M. – ISPRA http://www.isprambiente.gov.it/Media/carg/563_ISOLA_DI_SAN_PIETRO/Foglio.html.

Browne, P.R.L., 1978. Hydrothermal alteration in active geothermal fields. Rev. Earth Planet. Sci. 6, 229–250.

Catalano, R., Doglioni, C., Merlini, S., 2001. On the Mesozoic Ionian Basin. Geophys. J. Int. 144, 49–64.

Cherchi, A., Montadert, L., 1982. Oligo-Miocene rift of Sardinia and the early history of the Western Mediterranean Basin. Nature 298, 736–739.

Cioni, R., Salaro, L., Pioli, L., 2001. The Cenozoic volcanism of S. Pietro Island (Sardinia, Italy). In: Rend. Sem. Volume suppl., 71 (2), Facoltà Scienze Università Cagliari, pp. 149–163.

Conly, A.G., Scott, S.D., Bellon, H., 2011. Metalliferous manganese oxide mineralization associated with the Boléo Cu-Co-Zn district, Mexico. Econ. Geol. 106, 1173–1196.

Garbarino, C., Lirer, L., Maccioni, L., Salvadori, I., 1990. Isola di San Pietro Carloforte, cenni di geologia e vulcanologia – Edizione della Torre, Cagliari. 67, (in Italian).

Gisbert, G., Gimeno, D., 2016. Ignimbrite correlation using whole-rock geochemistry: an example from the Sulcis (SW Sardinia, Italy). Geol. Mag. 154, 740–756.

Grant, J.A., 1986. The isocon diagram—a simple solution to Gresens' equation for metasomatic alteration. Econ. Geol. 81, 1976–1982.

Gresens, R.L., 1967. Composition-volume relationship of metasomatism. Chem. Geol. 2, 47–55.

Guerin, H., 1983. Origine volcanologènedes gites manganésifères de Sardaigne. Bull. Soc. Geol. Fr. 25, 433–436.

Halbach, P., Friedrich, G., Von Stackelberg, U., 1988. The Manganese Nodule Belt of the Pacific Ocean Geological Environment, Nodule Formation, and Mining Aspects. Enke Verlag, Stuttgart 1988, (245 pp).

Hart, S.R., 1984. A large-scale isotope anomaly in the southern hemisphere mantle. Nature 309, 753–757.

Hein, J.R., Koschinsky, A., 2013. Deep-ocean ferromanganese crusts and nodules. In: Holland, H.D., Turekian, K.K. (Eds.), Treatise on Geochemistry, 2nd ed., vol. 13, Elsevier, Amsterdam, pp. 273–291, (Chapter 11).

Hein, J.R., Koschinsky, A., Halbach, P., Manheim, F.T., Bau, M., Kang, J.-K., Lubik, N., 1997. Iron and manganese oxide mineralization in the Pacific. In: Nicholson, K., Hein, J.R., Bühn, B., Dasgupta, S. (Eds.), Manganese Mineralization: Geochemistry and Mineralogy of Terrestrial and Marine Deposits. 119, Geological Society of London Special Publ, pp. 123–138.

Holster, W.T., 1997. Evaluation of the application of rare-earth elements to paleoceanography. Palaeogeogr. Palaeoclimatol. Palaeoecol. 132, 309–323.

Josso, P., Pelleter, E., Pourret, O., Fouquet, Y., Etoubleau, J., Cheron, S., Bollinger, C., 2017. A new discrimination scheme for oceanic ferromanganese deposits using high field strength and rare earth elements. Ore Geol. Rev. 87, 3–15.

Kilias, S.P., Naden, J., Cheliotis, I., Shepherd, T.J., Constandinidou, H., Crossing, J., Simos, I., 2001. Epithermal gold mineralization in the active Aegean volcanic arc: the Profitis Ilias deposit, Milos Island, Greece. Mineral. Deposita 36, 32–44.

Lezzerini, M., Tamponi, M., Bertoli, M., 2013. Reproducibility, precision and trueness of X-ray fluorescence data for mineralogical and/or petrographic purposes. Atti Soc. Tosc. Sci. Nat. Mem. Ser. A. 120, 67–73.

Lezzerini, M., Tamponi, M., Bertoli, M., 2014. Calibration of XRF data on silicate rocks using chemicals as in-house standards. Atti Soc. Tosc. Sci. Nat. Mem. Ser. A. 121, 65–70.

Liakopoulos, A., Glasby, G.P., Papavassiliou, C.T., Boulegue, J., 2001. Nature and origin of the Vanimanganese deposit, Milos, Greece: an overview. Ore Geol. Rev. 18, 181–209.

Lustrino, M., Melluso, L., Morra, V., 2000. The role of lower continental crust and lithospheric mantle in the genesis of Plio-Pleistocene volcanic rocks from Sardinia (Italy). Earth Planet. Sci. Lett. 180, 259–270.

Lustrino, M., Morra, V., Melluso, L., Brotzu, P., D'Amelio, F., Fedele, L., Franciosi, L., Lonis, R., Petteruti Liebercknecht, M.A., 2004. The Cenozoic igneous activity of Sardinia. In: Per. Mineral. 79, pp. 105–134.

Lustrino, M., Morra, V., Fedele, L., Serracino, M., 2007. The transition between "orogenic" and "anorogenic" magmatism in the western Mediterranean area: the Middle Miocenevolcanic rocks of isola del Toro (SW Sardinia, Italy). Terra Nova 19, 148–159.

Lustrino, M., Fedele, L., Melluso, L., Morra, V., Ronga, F., Geldmacher, J., Duggen, S., Agostini, S., Cucciniello, C., Franciosi, L., Meisel, T., 2013. Origin and evolution of Cenozoic magmatism of Sardinia (Italy). A combined isotopic (Sr-Nd-Pb-O-Hf-Os) and petrological view. Lithos 180–181, 138–158.

Lykakis, N., Kilias, S.P., 2010. Epithermal manganese mineralization, Kimolos island, South Aegean volcanic arc, Greece. Bull. Geol. Soc. Greece 43, 2646–2656.

McDonough, W.F., Sun, S.S., 1989. Chemical and isotopic systematics of oceanic basalts: implications for mantle composition and processes. Geol. Soc. Lond. Spec. Publ. 42, 313–345.

McLennan, S.M., 1989. Rare earth elements in sedimentary rocks: influence of provenance and sedimentary processes. Rev. Mineral. Geochem. 21, 169–200.

Mongelli, G., Mameli, P., Oggiano, G., Sinisi, R., 2013. Generation of Ce anomalies in SW Sardinian Mn ores. J. Geochem. Explor. 133, 42–49.

Moore, M.D., Reynolds, R.C., 1997. X-ray Diffraction and the Identification and Analysis of Clay Minerals. Oxford University Press, Oxford-New–York, (400 pp).

Mundula, F., Cioni, R., Rizzo, R., 2009. A simplified scheme for the description of textural features in Welded Ignimbrites: the example of San Pietro Island (Sardinia, Italy). Italian J. Geosci. 128, 615–627.

Naden, J., Kilias, S.P., Darbyshire, D.P.F., 2005. Active geothermal systems with entrained seawater as modern analogs for transitional volcanic-hosted massive sulfide and continental magmato-hydrothermal mineralization: the example of Milos Island, Greece. Geology 33, 541–544.

Nicholson, K., 1992. Contrasting mineralogical-geochemical signatures of manganese oxides: guides to metallogenesis. Econ. Geol. 87, 1253–1264.

Palomba, M., Padalino, G., Marchi, M., 2006. Industrial mineral occurrences associated with Cenozoic volcanic rocks of Sardinia (Italy): geological, mineralogical, geochemical features and genetic implications. Ore Geol. Rev. 29, 118–145.

Papavassiliou, K., Voudouris, P., Kanellopoulos, C., Glasby, G., Alfieris, D., Mitsis, I., 2017. New geochemical and mineralogical constraints on the genesis of the Vani hydrothermal manganese deposit at NW Milos island, Greece: comparison with the Aspro Gialoudi deposit and implications for the formation of the Milos manganese mineralization. Ore Geol. Rev. 80, 594–611.

Pattan, J.N., Pearce, N.J.G., Mislankar, P.G., 2005. Constraints in using Cerium anomaly of bulk sediments as an indicator of paleo bottom water redox environment: a case study from the Central Indian Ocean Basin. Chem. Geol. 221, 260–278.

Pioli, L., Rosi, M., 2005. Rheomorphic structures in a high-grade ignimbrite: the Nuraxi tuff, Sulcis volcanic district (SW Sardinia, Italy). J. Volcanol. Geotherm. Res. 142, 11–28.

Pirajno, F., 1992. Hydrothermal mineral deposits. In: Principles and Fundamental Concepts for the Exploration Geologist. Springer-Verlag, (709 pp).

Pourret, O., Davranche, M., Gruau, G., Dia, A., 2008. New insights into cerium anomalies in organic-rich alkaline waters. Chem. Geol. 251, 120–127.

Roy, S., 1992. Environments and processes of manganese deposition. Econ. Geol. 87, 1218–1236.

Roy, S., 1997. Genetic diversity of manganese deposition in the terrestrial geological record. In: Nicholson, K., Hein, J., Bühn, B., Dasgupta, S. (Eds.), Manganese Mineralisation: Geochemistry and Mineralogy of Terrestrial and Marine Deposits. vol. 119, Geological Society of London Special Publ, pp. 5–27.

Roy, S., 2006. Sedimentary manganese metallogenesis in response to the evolution of the Earth system. Earth Sci. Rev. 77, 273–305.

Ruggieri, G., Lattanzi, P., Luxoro, S.S., Dessì, R., Benvenuti, M., Tanelli, G., 1997. Geology, mineralogy and fluid inclusion data of the Furtei high-sulfidation gold deposit, Sardinia, Italy. Econ. Geol. 92, 1–19.

Schiffman, P., Fridleifsson, G.O., 1991. The smectite-chlorite transition in drillhole NJ-15, Nesjavellir geothermal field, Iceland: XRD, BSE and electron microprobe investigations. J. Metamorph. Geol. 9, 679–696.

Schmidt, K., Bau, M., Hein, J., Koschinsky, A., 2014. Fractionation of the geochemical twins Zr-Hf and Nb-Ta during scavenging from seawater by hydrogenetic ferromanganese crusts. Geochim. Cosmochim. Acta 140, 468–487.

Sinisi, R., Mameli, P., Mongelli, G., Oggiano, G., 2012. Different Mn-ores in a continental arc setting: Geochemical and mineralogicasl evidences from Tertiary deposits of Sardinia (Italy). Ore Geol. Rev. 47, 110–125.

Speranza, F., Villa, I.M., Sagnotti, L., Florindo, F., Cosentino, D., Cipollari, P., Mattei, M., 2002. Age of the Corsica-Sardinia rotation and Liguro-Provencal basin spreading: new paleomagnetic and Ar/Ar evidence. Tectonophysics 347, 231–251.

Stumpf, R., Frank, M., Schonfeld, J., Haley, B., 2010. Late Quaternary variability of Mediterranean outflow water from radiogenic Nd and Pb isotopes. Quat. Sci. Rev. 29, 2462–2472.

Surya Prakash, L., Ray, D., Paropkari, A.L., Mudholkar, A.V., Satyanarayanan, M., Sreenivas, B., Chandrasekharam, D., Kota, D., Kamesh Raju, K.A., Kaisary, S., Balaram, V., Gurav, T., 2012. Distribution of REEs and yttrium among major geochemical phases of marine Fe–Mn-oxides: comparative study between hydrogenous and hydrothermal deposits. Chem. Geol. 312–313, 127–137.

Xiao, J.F., He, J.Y., Yang, H.Y., Wu, C., 2017. Comparison between Datangpo-type manganese ores and modern marine ferromanganese oxyhydroxide precipitates based on rare earth elements. Ore Geol. Rev. 89, 290–308.